High-Energy Multiparticle Reactions*

W. R. FRAZER, L. INGBER, C. H. MEHTA, C. H. POON, D. SILVERMAN,† K. STOWE, P. D. TING, H. J. YESIAN‡

Department of Physics, University of California, San Diego, La Jolla, California 92037

(*June, 1971*)

(Revised January 1972)

Hadronic multiparticle reactions at very high energies are reviewed with emphasis on current theoretical pictures and models.

CONTENTS

I. INTRODUCTION

The motivation for this review grew out of the feeling that the field of multiparticle reactions is growing increasingly coherent, and increasingly likely to yield fundamental information about the nature of hadrons. Widespread agreement has developed as to some important questions to be asked of the experimental data, and excitement increases as partial answers to some of these questions become available. Nevertheless, it seemed to us as we began this work that this excitement was not widely shared among particle physicists, much less among the larger physics community. For example, despite their simplicity, single-particle inclusive spectra were explored very little even at existing accelerator energies. Two new facilities are or soon will be in operation: the CERN–ISR, intersecting storage rings providing proton–proton collisions at up to 60 GeV center of mass energy (the equivalent of 1900 GeV lab energy impinging on a stationary proton); and the NAL accelerator providing a proton beam at energies up to 500 GeV. We hope that this review will provide background material useful in the interpretation of data from these machines.

We begin, in Sec. II, with general features of multiparticle reactions, trying to emphasize considerations which are not tied to specific models. If this review should have any effect on future choices of measurements to be made, we would like it to help "maximize the possibility that the experimental data collected will remain useful despite continuing changes in theoretical fashions."[1] We defer to Sec. III the description of specific models, very obviously influenced in our choice by current theoretical trends. In Sec. IV we summarize the predictions of these models, as well as the more general considerations of Sec. II, and attempt a comparison with emphasis on those experiments which discriminate most effectively between models.

Although we have tried to emphasize general considerations and have tried to give an adequate presentation of other models, we caution the reader that all of us are theorists, and that we have among us invested several man years in the study of the multiperipheral model. This paper is primarily theoretical; the experimental data presentation is illustrative, not exhaustive.

Conversations with our colleagues over the course of the past few years were of course essential to the formation of this review, but it is impossible to enumerate them all. Some of the most extensive and recent help has come from J. S. Ball, T. Betlach, G. F. Chew, T. Ferbel, S. C. Frautschi, R. L. Lander, B. W. Lee, A. Mueller, R. Sugar, C. I. Tan, L. Van Hove, and L. L. Wang. Finally, the detailed criticism of our Editor, J. D. Jackson, led to most of the improvements in this revised manuscript.

We conclude this introduction with a guide to some of the other reviews of multiparticle hadronic reactions which have appeared recently, and which, because of their differing emphases, will help the reader to ob-

* This work was supported in part by the U.S. Atomic Energy Commission.

† Present address: Department of Physics, University of California, Irvine.

‡ Present address: Department of Physics, University of California, Berkeley.

[1] K. G. Wilson (1970).

tain a balanced picture of the field. Lander (1971), augmented by Krisch (1971), provides comprehensive coverage of data on inclusive reactions as of September 1971. A brief phenomenological review was given by Frazer (1971a), and a more comprehensive one by Berger (1971). Theoretical reviews with very different emphasis from the present one are those by Van Hove (1971) and Bjorken (1971). Reviews which very considerably overlap this one are those of Frazer (1971b), Quigg (1971), and Arnold (1971). Older reviews which have been useful to us are Wroblewski (1970a), Czyzewski (1968), and the entire proceedings of the International Conference on Expectations for Particle Reactions at New Accelerators (Madison, 1970) and of the 1969 Stony Brook Conference [*High Energy Collisions*, edited by C. N. Yang *et al.* (Gordon and Breach, New York, 1969)].

II. GENERAL FEATURES OF MULTIPARTICLE REACTIONS

A. Some Very General Observations

Two empirical rules concerning the nature of multiparticle reactions are so well accepted and so influential in both phenomenology and the construction of models as to deserve priority of presentation. They are

(1) *Smallness of transverse momenta*: The number of particles produced falls off very rapidly as a function of $q_\perp$, the magnitude of momentum transverse to the incident beam (compatible with exponential or Gaussian fits). The average value, $\langle q_\perp \rangle \approx 0.3$ to 0.4 GeV/c, is approximately independent of the incident energy, and does not depend strongly on the type of particle or multiplicity of particles produced. See, for example, Smith *et al.* (1969) or Elbert *et al.* (1968).

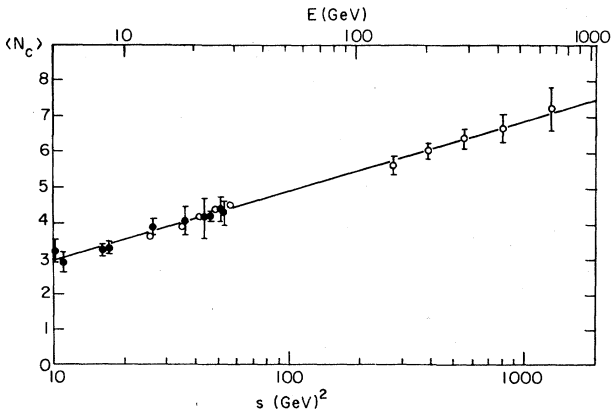

FIG. 2.1. Average multiplicity of charged secondaries as a function of energy in the Echo Lake cosmic ray experiment (Jones, 1970). High-energy points ($s>200$) are cosmic ray data; low-energy points are accelerator data.

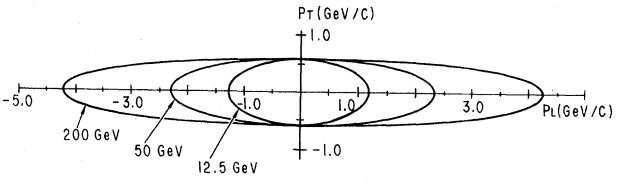

FIG. 2.2 Contours of constant cross section as a function of longitudinal and transverse momentum of secondary particle, for various beam momenta in $pp \to \pi^- X$. The contour at 12.5 GeV/c is taken from Akerlof *et al.* (1971); the others are estimated.

(2) *Low multiplicity of particles produced*: The average number of particles produced grows slowly with energy—much more slowly than would be the case if most of the available energy were converted into particles. The data on the multiplicity of charged particles from the Echo Lake cosmic ray experiment (Jones, 1970) shown in Fig. 2.1 are well fit by a logarithmic increase with energy

$$\langle n_{ch} \rangle = A + B \ln s, \tag{2.1}$$

where the values of the parameters for this and other similar fits are given in Table 2.1.

We shall return in Sec. II.F to a more detailed description of multiplicity distributions, but at the moment we are mainly concerned with observing that the multiplicity of particles produced is growing much less rapidly than the available energy would allow. This fact, together with the rule of smallness of transverse momenta, implies that most of the available energy goes into longitudinal motion (along the incident beam direction), and the average longitudinal momentum increases rapidly with incident energy,

$$\langle q_{||} \rangle \propto s^{1/2}/\ln s \gg \langle q_\perp \rangle. \tag{2.2}$$

Figure 2.2 sketches the elongation in $q_{||}$ of a typical contour of constant cross section as s increases. Thus the longitudinal momenta are the only variables which change rapidly with energy, and great kinematical simplifications can be obtained by recognizing this fact, as we shall discuss in the next sections.

B. Longitudinal Kinematics

1. *Longitudinal and Transverse Momenta*

The kinematics of a many-particle system is generally quite involved. Great simplifications result, however, in the region of very high-energy scattering. As we have seen in the previous sections, the final-state particles of such scattering processes are characterized by small mean transverse momenta (~0.4 GeV/c), which become independent of the incident energy as the latter becomes large. This, as already noted, suggests a differential treatment for the longitudinal and transverse momentum dependence of the scattering am-

TABLE 2.1. Fits to the multiplicity data shown in Fig. (2.1). Entries labeled (+*HBC*) include low-energy data; others fit only to the Echo Lake points (Jones, 1970) at high energies. The energy unit for E_L, $s^{1/2}$, and Q is GeV. L. W. Jones, private communication.

$\langle n_{ch}\rangle$		A	B	χ^2	Degrees of freedom
$A+B \ln E_L$	(+*HBC*)	1.46±0.16	0.89±0.05	7.0	8
		0.91±1.78	0.96±0.33	0.08	3
$A+B \ln s$	(+*HBC*)	0.79±0.20	0.91±0.05	7.9	8
		0.28±2.00	0.97±0.33	0.08	3
$A+2B \ln Q$	(+*HBC*)	1.98±0.13	0.73±0.04	3.9	8
		0.94±1.77	0.89±0.30	0.07	3

plitude. That is, if q is the four-momentum of a final state particle, it can be conveniently represented as:

$$q=(E, \mathbf{q}_\perp, q_{||}), \quad q_{||}=q_z, \quad \mathbf{q}_\perp=(q_x, q_y) \qquad (2.3)$$

where the incident beam is chosen to be in the z direction, and where $E=(q_{||}^2+\mu^2)^{1/2}$, $\mu=(m^2+q_\perp^2)^{1/2}$, and m is the rest mass of the particle in question; μ is sometimes referred to as the longitudinal mass. If one ignores what happens in the transverse momentum plane, the problem essentially reduces to one dimension in ordinary space, and μ becomes the effective mass (for a given $|\mathbf{q}_\perp|$).

As emphasized above, it is expected that a great deal of information will be contained in the longitudinal phase space (LPS) alone. Indeed it was suggested by Van Hove (1969) that LPS plots might provide a suitable framework for the phenomenological analysis of experimental data and for comparison with known theoretical models. This plot has had some interesting applications, as will be reviewed presently.

2. *LPS Plot*

(*a*) *Theory.* The main difficulty in a multiparticle phase space plot is the large number of dimensions. In the LPS plot, one makes use of the smallness of $\langle q_\perp\rangle$ and its independence of the incident energy, and projects the distributions of events onto the longitudinal portion of the phase space, thus greatly reducing the dimensionality of the plot. In contrast to the Dalitz plot, the phase space volume element here is not a constant. Appropriate phase space factors should therefore be included in order to exhibit the net distribution of events due to the scattering matrix element.

We now present an outline of the LPS plot. Consider the process

$$A+B\to C_1+\cdots+C_n. \qquad (2.4)$$

For definiteness, we go to the center-of-mass frame. The momentum q^i of the particle C_i is now represented as:

$$q^i=(E_i, \mathbf{q}_\perp{}^i, q_{||}{}^i),$$

where

$$E_i{}^2=\mu_i{}^2+(q_{||}{}^i)^2, \qquad \mu_i{}^2=m_i{}^2+|\mathbf{q}_\perp{}^i|^2.$$

The conservation of four-momenta reads

$$\sum_1^n E_i=W, \qquad (2.5a)$$

$$\sum_1^n q_{||}{}^i=0, \qquad (2.5b)$$

$$\sum_1^n \mathbf{q}_\perp{}^i=0. \qquad (2.5c)$$

The space of longitudinal momenta $(q_{||}{}^1, \cdots, q_{||}{}^n)$ is called S_n,[2] and the hyperplane of points satisfying the constraint (2.5b) is called L_{n-1}. The latter includes as a subset all the points of the longitudinal phase space for a physical process.

In the approximation $\mu_i=0$ for every i, the energy constraint (2.5a):

$$\sum_1^n E_i=\sum_1^n |q_{||}{}^i|=W \qquad (2.5a')$$

describes a polyhedron H_{n-2} in L_{n-1}. For a physical event, $\{\mu_i\}$ are in general nonzero but small compared to $\{q_{||}{}^i\}$. Then, for a given set of values $\{\mu_i\}$, the energy constraint (2.5a) describes a hypersurface K_{n-2} which lies inside the polyhedron H_{n-2}. Here K_{n-2} deviates from H_{n-2} most significantly at the vertices and sides of lower dimensions of the latter, which correspond to points where some of the $\{q_{||}{}^i\}$ vanish. The deviation, however, is of order μ_k for $q_{||k}=0$, and is small compared to the over-all size, $\sim W$, of K_{n-2} or H_{n-2}.

To illustrate these, consider the case $n=3$. The plot is shown in Fig. 2.3. The point P with coordinates $(q_{||}{}^1, q_{||}{}^2, q_{||}{}^3)$ is also given by the circular coordinates (p, ω). They are related as:

$$\begin{aligned} q_{||}{}^1&=p\sin\omega, \\ q_{||}{}^2&=p[-\tfrac{1}{2}\sin\omega-(\sqrt{3}/2)\cos\omega], \\ q_{||}{}^3&=p[-\tfrac{1}{2}\sin\omega+(\sqrt{3}/2)\cos\omega]. \end{aligned} \qquad (2.6)$$

Note that $(q_{||}{}^1)^2+(q_{||}{}^2)^2+(q_{||}{}^3)^2=\frac{3}{2}p^2$.

As already noted, peripherality of scattering means

[2] One may also use scaled parameters, such as Feynman's $x_i=2q_{||}{}^i/s^{1/2}$.

that most events will concentrate near the boundary. A useful related plot is then the ω distribution:

$$dN'/d\omega = \int |M|^2 \delta^2(\sum \mathbf{q}_\perp{}^i) \prod_{i=1}^{3} d^2\mathbf{q}_\perp{}^i, \qquad (2.7)$$

where N' = number of events weighted according to phase space density [see Van Hove (1969)], and M is the scattering matrix element. The applications of these plots will be summarized below.

(*b*) *Longitudinal Phase Space Phenomenology.* To get some feeling for the nature of longitudinal phase space phenomenology let us look first at the simplest case, a three-body final state. Since the three longitudinal momentum variables in the center-of-mass system, $q_{||}{}^1$, $q_{||}{}^2$, and $q_{||}{}^3$ are subject to the constraint that their sum is zero, a two-dimensional plot with axes at 60° is appropriate. The variables and kinematical boundaries are shown in Fig. 2.3. The experimental distribution for $\pi^+p \to \pi^+\pi^0 p$ is shown in Fig. 2.4. Note the clustering of points near the boundary. The energy-conservation constraint, Eq. (2.5a), would require all points to lie on the boundary if the transverse momenta were zero. Thus we see the rule of small transverse momenta appearing in this plot. Note also that practically all events lie in the left half-plane, corresponding to the proton in the final state continuing in the same direction as the proton in the initial state. Continuing in the spirit of displaying only the dependence on longitudinal momenta, Van Hove reduces the two-dimensional plot of Fig. 2.4 to one dimension by projecting all events onto the boundary; that is, he plots the density of events as a function of the angle ω defined in Fig. 2.3 and in Eq. (2.6). Figure 2.5, taken from Bialas *et al.* (1969), shows some of these plots. Note the strong clustering of events which occur even after prominent resonance production has been excluded.

This clustering of events can easily be understood in terms of Pomeron exchange (diffractive dissociation). In Fig. 2.6 the possible Pomeron exchange diagrams contributing to the reactions of Fig. 2.5 are shown. The ordering of the final-state particle from top to bottom of a graph corresponds to the ordering of the labeling q_1, q_2, q_3 of their longitudinal momenta. Consider Fig. 2.6(a). The π^0 and the p come out together, which means that q_2 and q_3 are both negative. This occurs, as can be seen from Fig. 2.3, if $60° < \omega < 120°$, which is just where the clustering occurs in Fig. 2.5(a). The rest of the distributions can be understood in the same manner from the Pomeron-exchange graphs in Fig. 2.6.

One additional interesting fact emerges from Fig. 2.5(c) and Fig. 2.5(f). The relative weakness of the bumps in these reactions can be understood from the Gribov–Morrison rule of conservation of "naturality" [naturality $= (-1)^J P$]: This rule states that particles (or systems of particles) A and B couple to a Pomeron only if they have the same naturality.

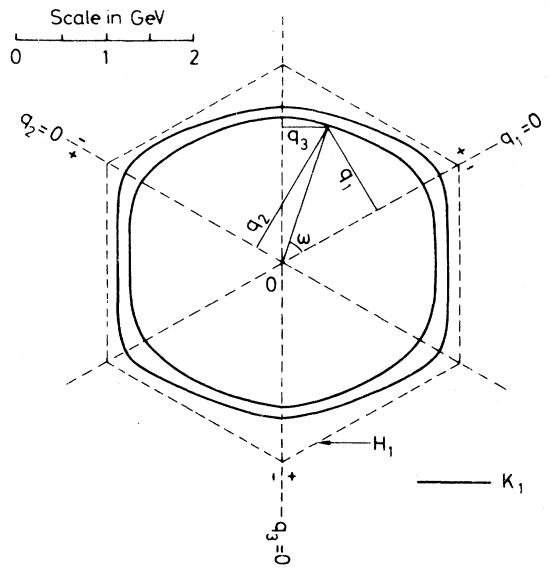

FIG. 2.3 Longitudinal phase space plot for $\pi\pi N$ at c.m. energy $W = 4$ GeV. The inner full curve is the boundary for typical transverse momenta, whereas the outer full curve is for zero transverse momenta. The dashed curve is the boundary in the zero mass, zero transverse momentum limit.

Elegant as the LPS plots are, it can still be argued that all the foregoing material could be seen on more conventional Dalitz or Chew–Low plots. With four-body final states the LPS plot clearly shows its utility. Here the LPS boundary is a polyhedron called a cuboctahedron. Just as the two-dimensional LPS plot for three-body final states is reduced to the one-dimensional plots of Fig. 2.5 by projection on the boundary, so are the four-body distributions two-dimensional after projection on the cuboctahedron.

The example of $\pi^-p \to 2\pi^-\pi^+p$ at 11 and 16 GeV/c has been analyzed by Kittel, Ratti, and Van Hove (1971). For this reaction the only region of the LPS plot with appreciable population is defined by $q_{||}{}^p < 0$, $q_{||}{}^f > 0$, where the superscripts p, $+$, f, and s refer to proton, π^+, and fast and slow π^-, respectively. The resulting distributions are shown in Fig. 2.7, where $q_{||}{}^+$ and $q_{||}{}^s$ are used as independent variables.

Two facts emerge clearly from the elegant display in Fig. 2.7: (1) Only the regions favored by Pomeron exchange are heavily populated (see Fig. 2.8 for the exchanges which populate the different regions). (2) In the heavily populated regions the density of events does not vary significantly from 11 to 16 GeV/c, which confirms the assignment of these events to Pomeron exchange. The LPS plot has shown us in a very clear and detailed manner that single Pomeron exhange (diffraction dissociation) is the dominant mechanism in the reactions studied. We shall return to this point later, since the comparison of the relative importance of diffractive

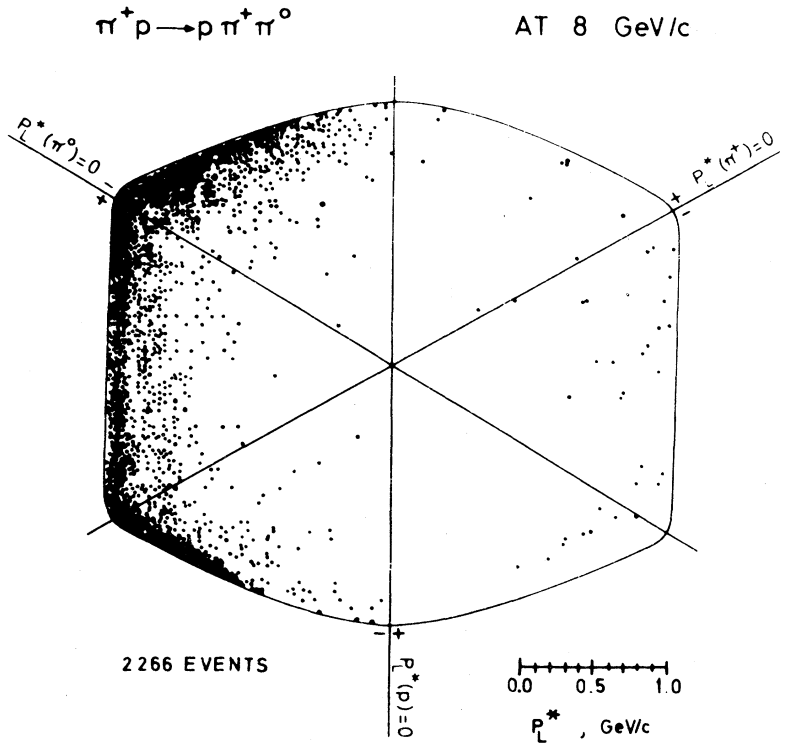

FIG. 2.4 Experimental LPS plot for $\pi^+p \to \pi^+\pi^0 p$ at 8 GeV/c, from Van Hove (1969).

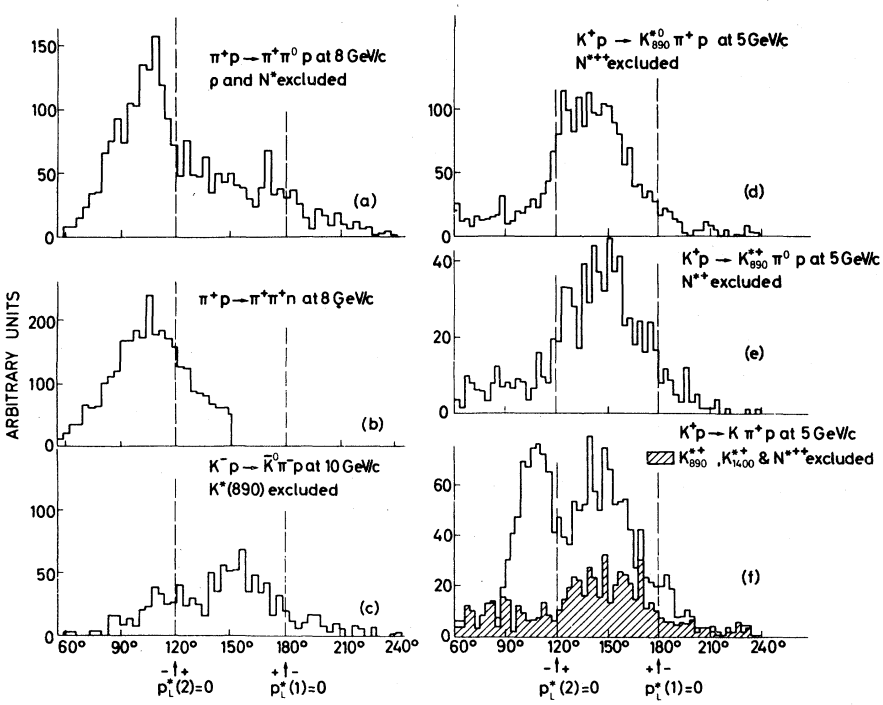

FIG. 2.5 Experimental LPS plots projected on the boundary, as a function of the polar angle ω, weighted by the longitudinal phase space (Białas, 1969). See Fig. 2.3 for definition of ω. Momenta q_1, q_2, q_3 are assigned to particles in the order in which they are written on figure.

vs multiperipheral production is one of the important issues to be resolved.

In this section, however, we are most interested in assessing the value of the LPS plot as a phenomenological tool. The example we have discussed establishes its value for four-body final states. Kittel, Ratti, and Van Hove have also succeeded in using LPS plots to extract interesting features of five-body production reactions, but here the fact that the plot is three-dimensional makes it much harder to read. Obviously, simpler displays, such as single-particle densities and two-particle correlations, are needed for higher multiplicities. These will be discussed in succeeding sections.

Before leaving this subject of LPS plots, it may be worthwhile to discuss their significance from a more general point of view: the LPS plot is an example of data presentation, relatively unbiased by theoretical models, in which one hopes to recognize patterns which elucidate the underlying physics. As the number of final-state particles grows, it becomes impossible to comprehend complete multivariable distributions. The important task of the phenomenologist is then the devising of useful ways to present these data. Bjorken (1971) has expressed the problem as one of devising "projection operators" to project the data onto spaces of manageable numbers of dimensions. Inclusive spectra, where only one or two final-state particle momenta are specified, are currently the most-used form of projection. Although we shall devote a large fraction of this review to discussion of inclusive spectra, we must recognize the incompleteness of this presentation and hope for the development of other, complementary, projections.

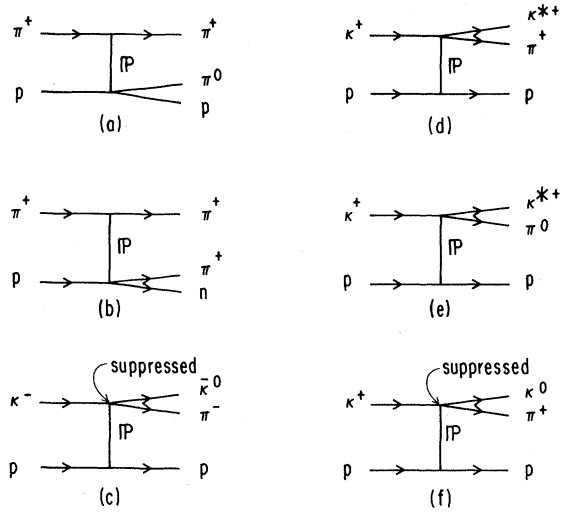

FIG. 2.6. Pomeron exchange diagrams by which the processes in Fig. 2.5 can be interpreted.

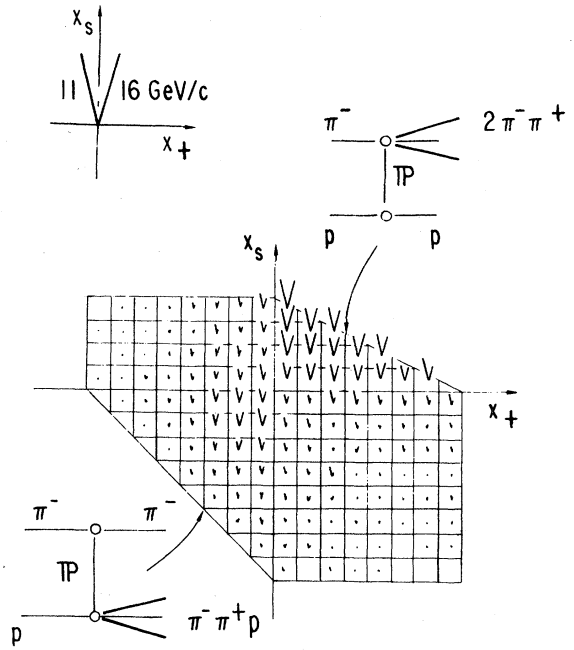

FIG. 2.7. LPS distributions for $\pi^- p \to 2\pi^-\pi^+ p$ at 11 and 16 GeV/c. The oblique segments drawn upward from the bin centers measure the number of events in each bin at 11 GeV/c (left-hand segment) and 16 GeV/c (right-hand segment). The graphs show the possible Pomeron exchange processes (Kittel, 1970).

3. *Choice of Longitudinal Variables*

The foregoing sections have emphasized the utility of distinguishing the role of longitudinal and transverse momenta. Models and phenomenological schemes generally make this distinction. Manifest covariance under general Lorentz transformations is thereby sacrificed, and only invariance under longitudinal Lorentz trans-

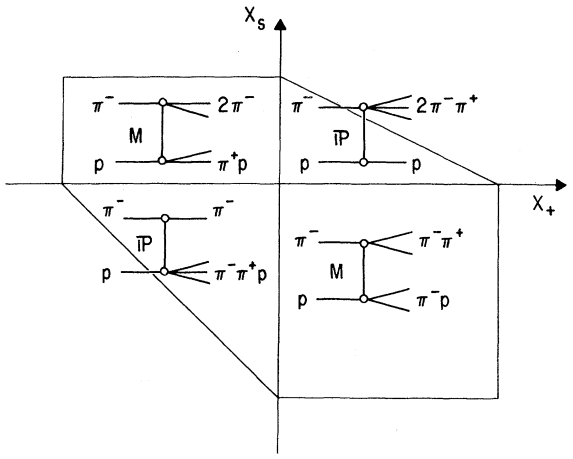

FIG. 2.8. Possible exchange diagrams contributing to the four regions of Fig. 2.7.

formations (transformations along the beam direction) remains. Under these transformations the tranverse momenta are invariant, and need no further discussion. The choice of a reference frame for the longitudinal momenta varies, however, according to the physical picture one favors. Benecke, Chou, Yang, and Yen (1969), picturing multiparticle production as a diffractive fragmentation of the projectile and target, favor the rest frames of these particles. Feynman (1969), picturing particle production by bremsstrahlung resulting from change of direction of a parton, prefers the center of mass system, in which the bremsstrahlung products would have relatively low energy. The multiperipheral model prefers no special frame, since it implies production of particles evenly spaced (on the average) in the parameter specifying the longitudinal Lorentz transformation.

There is one elegant choice of variable which eliminates the bias imposed on the data presentation by choice of a particular frame. This variable was used by Wilson in 1963 (Wilson, 1963), and has recently been employed by Feynman (1969), Van Hove (1971), and DeTar (1971).

Consider the process

$$p_a+p_b\rightarrow q^i+X, \tag{2.8}$$

where p_b is the beam four-momentum, p_a is the target four-momentum, q^i is the four-momentum of the ith outgoing particle, and X represents the rest of the outgoing particles. Specializing to the laboratory frame, we find $\mathbf{p}_a=0$. Then the rapidity y_i is defined as

$$y_i=\sinh^{-1}(q_{||}{}^i/\mu_i)=\tfrac{1}{2}\ln[(E_i+q_{||}{}^i)/(E_i-q_{||}{}^i)], \tag{2.9}$$

where the *longitudinal mass* μ_i is defined as

$$\mu_i=(m_i{}^2+|\,\mathbf{q}_\perp{}^i\,|^2)^{1/2}. \tag{2.10}$$

Often one can drop the superscript i when there is no confusion about which final particle is being considered. In terms of the rapidity y_i, the four-momentum q_i in the laboratory system is given by

$$q^i=(\mu_i\cosh y_i,\ q_x{}^i,\ q_y{}^i,\ \mu_i\sinh y_i), \tag{2.11}$$

where the z direction has been chosen along the beam, so that

$$\mathbf{q}_\perp{}^i=(q_x{}^i,\ q_y{}^i), \tag{2.12}$$

The rapidity y_i specifies the longitudinal Lorentz transformation that relates the lab frame to the frame in which particle i has zero longitudinal momentum.

All longitudinally moving frames are put on an equal footing by the use of the y_i variables, since they are all related by a simple shift of the scale. That is, a longitudinal Lorentz transformation characterized by $\gamma=\cosh u$ merely changes y_i to y_i', where $y_i'=y_i+u$.

The beam and target momenta are given by

$$p_b=(m_b\cosh y_b,\ 0,\ 0,\ m_b\sinh y_b).$$
$$p_a=(m_a,\ 0,\ 0,\ 0), \tag{2.13}$$

where $s=(p_a+p_b)^2$ is exponentially related to y_b in the large s limit

$$s\cong m_am_b\exp(y_b), \tag{2.14}$$

where the asymptotic equality refers to the region $s\gg m_a{}^2,\ m_b{}^2$.

The absolute kinematic limits on y for a fixed value of q are given in the asymptotic region by[3]

$$\ln(\mu/m_a)<y<y_b+\ln(m_b/\mu). \tag{2.15}$$

The total length of the kinematically allowed region in y is equal to Y, where

$$y_{\max}-y_{\min}Y=\ln(s/\mu^2). \tag{2.15b}$$

The length Y of the y plot varies with the type of particle observed, but not with the nature of beam or target particle. If one wishes to have a plot of constant length, one can use a reduced rapidity $y_r=y/Y$, which is asymptotically restricted to $0\leq y_r\leq 1$. This variable does, however, have the drawback that at infinite energy it maps any momentum which remains finite in the laboratory into the point $y_r=0$, and any momentum which remains finite in the projectile frame into the point $y_r=1$. This is analogous to the situation with the x variable, in which all finite momenta in the cm system are mapped into $x=0$. Mapping has always been a useful technique for the theorist, but in this field the judicious choice of variable offers us the unique opportunity to map the entire region in which our theories fail, into a single point!

We conclude this section by collecting the relations between the three common choices of longitudinal variables: y, $q_{||}$ (lab frame), and x, where we use the definition

$$x=2q_{||}{}^*/s^{1/2}. \tag{2.16}$$

An asterisk is used here to denote a c.m. quantity. Two other definitions are in common use, $x=q_{||}{}^*/p_a{}^*$ and $x=q_{||}{}^*/(q_{||}{}^*)_{\max}$, which differ slightly at finite s, but approach the same limit. Although the latter definition has the advantage of restricting x to exactly $-1<x<1$, it leads to complicated connections with other variables because of the dependence of $(q_{||}{}^*)_{\max}$ on the nature of the final state particles.[4]

The exact relation between $q_{||}$ in the lab frame and x is given by a Lorentz transformation,

$$q_{||}=\tfrac{1}{2}\sqrt{s}\,\{\sinh u[x^2+(4\mu^2/s)]^{1/2}+x\cosh u\}, \tag{2.17}$$

where $\mu^2=q_\perp{}^2+m^2$ and where $\sinh u=p_a{}^*/m_a$.

[3] This can be derived from Eq. (3.9).

[4] We doubt that it is worthwhile spending much time worrying over which x to use, and advocate standardizing to the simplest definition, Eq. (2.16). The differences are of the order $1/s$, and experience with two-body Regge phenomenology does not instill confidence in our ability to understand corrections of this order.

Expanding the square root one finds the asymptotic formulas

$$q_{||}=\tfrac{1}{2}m_a x-(\mu^2/2xm_a)+O(s^{-1}), \qquad x\ll-(2\mu/s^{1/2})$$
$$=sx/2m_a+O(1), \qquad x\gg(2\mu/s^{1/2}), \tag{2.18}$$

whereas at $x=0$, $q_{||}=\mu s^{1/2}/2m_a$.

The exact inverse relation is

$$x=(2/s^{1/2})[q_{||}\cosh u-(q_{||}^2+\mu^2)^{1/2}\sinh u]. \tag{2.19}$$

As long as $q_{||}$ is held fixed as $s\to\infty$, this gives the result

$$x=m_a^{-1}[q_{||}-(q_{||}^2+\mu^2)^{1/2}+O(s^{-1})]$$
$$=(q_{||}-E_q)/m_a+O(s^{-1}) \tag{2.20}$$

which is always negative. However, if $q_{||}$ grows as $s^{1/2}$ (to be specific, let $q_{||}=\eta s^{1/2}$), then one obtains

$$x\cong(4m_a^2\eta^2-\mu^2)/2\eta m_a s^{1/2}, \quad \text{if} \quad q_{||}=\eta s^{1/2}, \tag{2.21}$$

which vanishes as $s\to\infty$. Finally, if $q_{||}$ grows as fast as possible, as s, then one finds

$$x\cong r, \quad \text{if} \quad q_{||}=rs/2m_a. \tag{2.22}$$

Analogous relations hold in the projectile frame.

The relation between y and $q_{||}$ is just the definition of y, Eq. (2.9),

$$y=\sinh^{-1}(q_{||}/\mu). \tag{2.23}$$

The basic relation between x and y can be found by performing a Lorentz transformation to the c.m. system on the above equation, which yields

$$x=(2\mu/s^{1/2})\sinh y^*, \qquad y^*=y-u. \tag{2.24}$$

Taking a large-s limit yields

$$x\cong(\mu/m_a)[-e^{-y}+(m_a^2/s)e^{y}]. \tag{2.25}$$

The inverse relation is of the form

$$y=\ln(-\mu/xm_a), \qquad x\ll-(2\mu/s^{1/2}),$$
$$=\ln(xs/\mu m_a), \qquad x\gg 2\mu/s^{1/2}, \tag{2.26}$$

whereas $x=0$ corresponds to $y=u$.

The rapidity y^* defined in terms of c.m. momenta in terms of lab momenta is formally somewhat simpler than y. It is easy to see by adding and subtracting the energy–momentum conservation conditions

$$\sum q_{||}^{*i}=0, \qquad \sum q_0^{*i}=s^{1/2}$$

that

$$\sum\mu_i\exp(y_i^*)=s^{1/2}=\sum\mu_i\exp(-y_i^*).$$

From these equations it follows that the absolute limits on y^* are

$$-\tfrac{1}{2}Y_i<y_i^*<\tfrac{1}{2}Y_i, \tag{2.15a'}$$

where

$$Y_i=\ln(s/\mu_i^2). \tag{2.15b'}$$

The relationship of y^* to x is given by the definition,

TABLE 2.2. Relations among various sets of kinematic variables for single-particle inclusive reactions.

Reaction:

$$p_a+p_b\to q+X$$

masses m_a m_b m M

Definitions:

Momenta without superscripts refer to lab frame
Asterisks refer to c.m. frame
Superscript "b" refers to projectile rest frame

$q_{||}=q_z$, $+z$ direction along $\mathbf{p}_b$

$\mu^2\equiv q_\perp^2+m^2$, $\quad x\equiv 2q_{||}^*/s^{1/2}$

$y\equiv\sinh^{-1}(q_{||}/\mu)$, $\quad y^*\equiv\sinh^{-1}(q_{||}^*/\mu)$

$Y\equiv\ln(s/\mu^2)$

Exact relations, valid for all physical x, y, q_n:

$y^*=y-u$, $\quad \cosh u=E_a^*/m_a$, $\quad \sinh u=p_a^*/m_a$

$x=(2/s^{1/2})[q_{||}\cosh u-(q_{||}^2+\mu^2)^{1/2}\sinh u]$

$q_{||}=(s^{1/2}/2)\{x\cosh u+\sinh u[x^2+(4\mu^2/s)]^{1/2}\}$

$x=\exp(-\tfrac{1}{2}Y+y^*)-\exp(-\tfrac{1}{2}Y-y^*)$

$[x^2+(4\mu^2/s)]^{1/2}=1-[(M^2-m^2)/s]$

Approximate relations, valid for $x\ll-2\mu/s^{1/2}$

$q_{||}=\tfrac{1}{2}m_a[x-(\mu^2/xm_a^2)]+O(s^{-1})$

$x=[q_{||}-(q_{||}^2+\mu^2)^{1/2}]/m_a+O(s^{-1}, q_{||}/s)$

$q_{||}^b=sx/2m_b+O(1)$

$x=-\exp(-\tfrac{1}{2}Y-y^*)+O[\exp(-\tfrac{1}{2}Y+y^*)]$

$x=-1+(M^2/s)+O(\mu^2/xs)$

Approximate relations, valid for $x\gg(2\mu/s^{1/2})$

$q_{||}^b=\tfrac{1}{2}m_b[x-(\mu^2/xm_b^2)]+O(s^{-1})$

$x=\{q_{||}^b+[(q_{||}^b)^2+\mu^2]^{1/2}\}/m_b+O[s^{-1}, (q_{||}^b/s)]$

$q_{||}=sx/2m_a+O(1)$

$x=\exp(-\tfrac{1}{2}Y+y^*)+O[\exp(-\tfrac{1}{2}Y-y^*)]$

$x=1-(M^2/s)+O(\mu^2/xs)$

Eq. (2.24), which can be written in the form

$$x=\exp[-(\tfrac{1}{2}Y-y^*)]-\exp[-(\tfrac{1}{2}Y+y^*)]. \tag{2.25'}$$

Note that $\frac{1}{2}Y-y^*$ is the distance from y^* to the right-hand limit of the rapidity plot, and $\frac{1}{2}Y+y^*$ is the distance to the left-hand end. These formulas are collected in Table 2.2.

The Jacobians of these transformations can be read off from the Lorentz invariance of d^3q/E_q. Since $d^3q=d^2\mathbf{q}_\perp dq_{||}$, it follows that $dq_{||}/E$ is invariant under Lorentz transformations along the beam direction, and there-

fore that

$$dq_{||}/(q_{||}^2+\mu^2)^{1/2}=dx/[x^2+(4\mu^2/s)]^{1/2}=dy. \quad (2.27)$$

C. Inclusive Spectra; Scaling

1. Definitions and Conventions

Since the complete display of dependence on all the longitudinal momenta is impractical for more than five particles in the final state, experimenters and theorists have turned to simpler distributions. The first to be investigated is the single-particle inclusive spectrum; that is,

$$a+b\to c+X$$

with momenta

$$p_a+p_b=q+\cdots,$$

where X stands for whatever else is produced, but not observed. It is convenient to write the unpolarized cross section in terms of a function $F_{ab}^{c}(q_{||}, q_\perp, s)$ defined as:

$$E_q[d^3\sigma(ab\to c+X)/dq^3]\equiv F_{ab}^{c}(q_{||}, q_\perp, s) \quad (2.29)$$

where[5] $q_\perp=|\mathbf{q}_\perp|$. We shall frequently drop the sub and superscripts when they are not required for clarity.

We encourage everyone to use this invariant function F rather than $d^3\sigma/dq^3$. The factor E_q multiplies out an uninteresting phase space variation. The current situation in which some data are presented with the E factor and some without this factor makes comparisons difficult. At the time of this writing, however, the confusion still persists. If we cannot agree on such a simple thing as invariant phase space, perhaps we could at least agree to present data *in bins* in $q_\perp$, rather than presenting only averages over all $q_\perp$. Then readers could convert to their own favorite plots.

Multiparticle inclusive spectra can also be defined. Neither experiment nor theory has progressed beyond the two-particle inclusive reaction,

$$a+b\to c_1+c_2+X$$

for which the two-particle inclusive spectrum is defined as

$$E_1E_2[d^6\sigma(ab\to c_1+c_2+X)/d^3q_1d^3q_2]\equiv F_{ab}^{(2)c_1c_2}(\mathbf{q}_1, \mathbf{q}_2, s). \quad (2.30)$$

Many theoretical results simplify when expressed in terms of *densities* $\rho^{(n)}$ rather than in spectra $F^{(n)}$, where the densities are defined by dividing by the total cross section σ_{ab},

$$\rho_{ab}^{(n)c_1c_2\cdots c_n}\equiv(1/\sigma_{ab})F_{ab}^{(n)c_1c_2\cdots c_n}. \quad (2.31)$$

Since we shall most often discuss the single-particle density, we abbreviate by simply writing ρ for $\rho^{(1)}$.

[5] More general $\mathbf{q}_\perp$ dependence is of course permitted in polarized reactions, which we do not consider here.

2. Normalization and Sum Rules

Since an event with n particles in the final state is counted n times in a single-particle inclusive measurement, it follows that

$$\int(d^3q/E_q)\rho(\mathbf{q}, s)=\langle n\rangle, \quad (2.32)$$

where the average multiplicity $\langle n\rangle$ is

$$\langle n\rangle=\sigma_{\text{tot}}^{-1}\sum n\sigma^{(n)}. \quad (2.33)$$

Caution: Experimenters often normalize $\langle n\rangle$ to the inelastic instead of the total cross section by excluding elastic events from measurement.

If the experiment measures only particles of a given type, π^- for example, then the normalization is

$$\int(d^3q_c/E_c)\rho_c=\langle n_c\rangle \quad (2.34)$$

where the subscript c labels the particle type. The two-particle inclusive density satisfies the normalization

$$\int(d^3q_c/E_c)(d^3q_d/E_d)\rho^{(2)}(\mathbf{q}_c, \mathbf{q}_d, s)=\langle n_cn_d-n_c\delta_{cd}\rangle. \quad (2.35)$$

Useful sum rules can be derived by integrating inclusive densities multiplied by components of momenta (Chou, 1970; DeTar, 1971c). The simplest of these is an expression of energy conservation,

$$\sum_c\int d^3q\rho_c(\mathbf{q}, s)=s^{1/2} \quad (2.36a)$$

which can also be written in the form

$$\sum_c\int_{-1}^{1}dx\int d^2q_\perp\rho_c(x, q_\perp, s)=2. \quad (2.36b)$$

3. Limiting Fragmentation and Scaling

Organization of the data on single-particle spectra has been greatly facilitated by the *scaling* and *limiting fragmentation* hypotheses. These hypotheses have a long history, starting with the pioneering work of Amati, Fubini, and Stanghellini (1962). Wilson (1963) was the first to recognize the generality of the scaling idea, but its importance was not widely appreciated until its rediscovery by Feynman (1969) and Benecke, Chou, Yang, and Yen (1969). We shall present the various forms of the scaling/limiting-fragmentation hypothesis, and discuss the degree to which they are equivalent and the extent to which they are confirmed by current data. We shall first state the hypothesis with only a sketch of one of the several pictures of high-energy phenomena which imply it. Another picture, that of short-range correlations, will be developed in the next section. It is remarkable that theorists using such a variety of pictures of high-energy phenomena agree on the same conclusion. In Feynman's words, "I am more sure of the conclusions than of any single argument which suggested them to me, for they have an internal consistency which surprises me and exceeds

the consistency of my deductive arguments which hinted at their existence" (Feynman, 1969).

Limiting fragmentation hypothesis. In this form, proposed by Benecke, Chou, Yang, and Yen (BCYY), one uses either the laboratory or projectile rest frame. In the laboratory, for example, the hypothesis is that $F(q_{||}, q_\perp, s)$ approaches an asymptotic limit for large s

$$F(q_{||}, q_\perp, s) \cong F(q_{||}, q_\perp) \tag{2.37}$$

provided that $q_{||}$ is held fixed as $s \to \infty$. Such particles are considered by BCYY as *fragments* of the *target*. A similar statement holds in the projectile rest frame, which we denote by the superscript b,

$$\rho(q_{||}{}^b, q_\perp, s) \cong \rho(q_{||}{}^b, q_\perp) \tag{2.38}$$

provided that $q_{||}{}^b$ is held fixed as $s \to \infty$. Similar statements are also hypothesized for two- and more-particle distributions.

One argument given by BCYY for this hypothesis is based on the geometrical picture of Yang and collaborators. In the lab system, the projectile Lorentz contracts into a thin disk which passes through the target and excites it. "What is the effect of higher and higher projectile momentum? The time of passage is essentially fixed, but the disk is further and further compressed. The constancy of the total cross section and of the elastic scattering cross section suggest that the momentum and quantum-number transfer process between the 'stuff' in the projectile and the 'stuff' in the target does not appreciably change when the projectile is further and further compressed. Thus one expects that the excitation and breakup of the target approaches a limiting distribution" (Benecke, 1969).

Scaling hypothesis. In this form, proposed by Feynman, one regards $F(q_{||}{}^*, q_\perp, s)$ as a function of c.m. variables, which we denote by asterisks. The scaling hypothesis then says that asymptotically in s the function $F(q_{||}{}^*, q_\perp, s)$ depends only on $q_\perp$ and $x = 2q_{||}{}^*/s^{1/2}$,

$$F(q_{||}{}^*, q_\perp, s) \cong \tilde{F}(x, s). \tag{2.39}$$

For $x^2 \gg 4\mu^2/s$, this is equivalent to the hypothesis of limiting fragmentation. From Eq. (2.20) one sees that for $x \ll -2\mu/s^{1/2}$, fixed x implies fixed $q_{||}$ in the lab; similarly, for $x \gg 2\mu/s^{1/2}$, fixed x implies fixed $q_{||}{}^b$ in the projectile rest frame. However, the point $x=0$ does not correspond to any finite momentum in the lab or projectile frame, but instead to finite momentum in the cm system. Thus scaling includes the limiting fragmentation hypothesis, but goes beyond it in making a statement about the region $x \approx 0$ also. In this *central region* Feynman makes the further prediction, based on a bremsstrahlung picture, that $F(x, q_\perp)$ should be independent of x for small x.[6] We discuss this prediction in more detail in the next section, from the point of view of short-range correlations in the rapidity variable y.

Experimental results on limiting fragmentation. Since the importance of the scaling/limiting fragmentation hypotheses has only recently come to be appreciated, there were very little relevant data available at the time of writing of the first draft of this review. In the meantime, fashions have changed to such an extent that it is impossible for us to present a comprehensive review of the data. Of the medium-energy data (<30 GeV), which is summarized in Lander's review (1971), we present only one example: $pp \to \pi^- X$ at five energies from 13 to 28 GeV (D. Smith, 1971), shown in Fig. 2.9. Both the $q_{||}$ and $q_\perp$ distributions show little variation over this energy range.

The successful operation of the intersecting storage rings (ISR) at CERN has opened up a vast new energy range in pp reactions. Figure 2.10 (Krisch, 1971; Ratner, 1971) shows that limiting fragmentation passed the test, within presently available accuracy! Note, however, that scaling in the central region is still untested, a point to which we return in the next section.

Limiting fragmentation has now passed its first tests, and the utility of the idea is confirmed. The study of the nature of the limiting behavior of single-particle inclusive spectra will now become more refined, yielding information on the approach to the limit which will greatly enrich our knowledge gained through study of total cross sections, the simplest of inclusive reactions.

D. Short-Range Correlation Picture

1. Correlation Length Hypothesis

We present in this section a picture of high-energy phenomena which provides an intuitively simple motivation for the scaling hypothesis discussed in the previous section, but which is powerful enough to lead to many additional predictions. Wilson (1963) was the first to see that the predictions of the multiperipheral model concerning the single-particle inclusive spectra depended only on rather general hypotheses: (a) limited transverse momenta, and (b) short-range order in longitudinal momenta. DeTar (1971) and Wilson (1970) have explored this observation more fully. Although it has been abstracted from multipheripheral models, and includes all their most successful predictions, it is more general than any specific model and is therefore presented here. Discussion of specific multiperipheral models can be found in Sec. III.A.

Since the transverse momenta are limited to small values, we shall ignore them and concentrate as before on the distributions in $q_{||}$; or, more conveniently, the lab rapidity $y = \sinh^{-1}(q_{||}/\mu)$, where $\mu^2 = m^2 + q_\perp{}^2$ (see Sec. II.B.3 for a discussion of these variables).

The *correlation length hypothesis* states that there is no correlation between particles whose rapidities y_i are

[6] This prediction has a long history. It was found by Amati, Fubini, and Stanghellini (1962) to be a consequence of the multiperipheral model. Heisenberg (1963) saw it as a consequence of the Lorentz contraction of the source region of overlap of the target and projectile disks in the c.m. system.

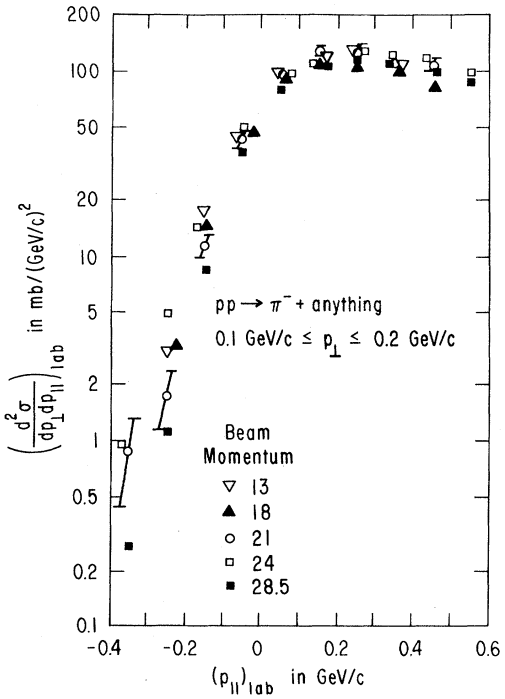

(a)

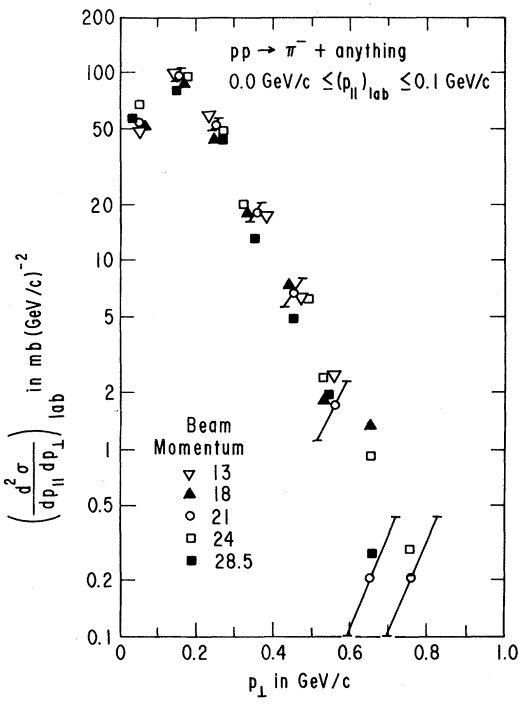

(b)

FIG. 2.9. Test of limiting distribution hypothesis in single-particle inclusive spectrum of $p\bar{p} \to \pi^- +$anything at various beam energies. Points at different energies should coincide if distribution is limiting. (a) Longitudinal momentum spectrum, (b) transverse momentum spectrum.

separated by a distance large compared to a certain *correlation length* L; that is, for $|y_i - y_j| \gg L$. Moreover, there is no correlation with the incident particles as long as their rapidities y_a and y_b differ from y by a distance large compared to L. With rapidities defined in the laboratory frame, this means that the outgoing particle will have no correlation with the target as long as $y \gg L$, and no correlation with the projectile for $y \ll Y-L$.[7] We shall now show that all the predictions we have encountered previously follow from this correlation length hypothesis.[8]

Consider the hypothetical single-particle spectrum shown in Fig. 2.11. It is divided into three regions: Region T, which we call the *target fragmentation* region, where $y<L$; Region C, the *central region*, where $L<y<Y-L$; and the *beam fragmentation* region, where $y>Y-L$. Consider first the target fragmentation region. The single-particle spectrum depends on only three variables, which we take to be $q_\perp$, y, and $y-Y$. But assuming high enough energy that $Y \gg 2L$, then in the target fragmentation region $Y-y \gg L$, dependence on this variable would violate the correlation length hypothesis. Therefore, we have

$$(E_q/\sigma_{ab})(d^3\sigma_{ab}{}^c/dq^3) \equiv \rho_{ab}{}^c(q_\perp, y, y-Y) \cong \rho_{ab}{}^c(q_\perp, y) \quad \text{for } Y-y \gg L. \quad (2.40)$$

That is, the distribution is limiting. Moreover, there can be no correlation with the beam particle (except for a normalizing factor), so the distribution reduces to

$$\rho_{ab}{}^c(q_\perp, y, y-Y) \cong \gamma_a{}^c(q_\perp, y) \quad \text{for } Y-y \gg 2L. \quad (2.41)$$

In the beam fragmentation region, the corresponding result is

$$\rho_{ab}{}^c(q_\perp, y, y-Y) \cong \gamma_b{}^c(q_\perp, y-Y) \quad \text{for } y \gg L. \quad (2.42)$$

In the central region, both y and $y-Y$ are large compared to L, so that the spectrum must be independent of both, and independent of the nature of both target and projectile,

$$\rho_{ab}{}^c(q_\perp, y, y-Y) \cong \gamma^c(q_\perp) \quad \text{for } L \ll y \ll Y-L. \quad (2.43)$$

[7] There is no compelling reason to believe that all these correlations lengths are the same, but we shall use one symbol for simplicity. Also, in order to simplify kinematic relations in Table 2.2, we defined Y as the total length of the rapidity plot, $Y = \ln(s/\mu^2)$, rather than defining $Y = y_b$ as DeTar (1971) does. The fact that $Y \neq y_b$ in general means that y_a and y_b are not quite at the ends of the rapidity plot. We know of no physical reason to attach greater signficance to discussion of correlations in terms of distances from y_b and y_a, or in terms of distances from the ends of the plot. Therefore, we ignore differences of this order, and choose on the basis of notational simplicity.

[8] This picture has been discussed by Feynman and by Wilson (1970) in terms of the analogy with a gas or liquid. Coordinates of each particle in the liquid are the two components of transverse momentum and the rapidity. Since $\langle q_\perp \rangle$ is small, independent of energy, the liquid is confined to a long thin cigar-shaped volume as in Fig. 2.2. The single-particle density $\rho^{(1)}$ is the density of the liquid. Correlations are short-range, both among the particles of the liquid and between the particles and the walls.

This equation predicts a *central plateau* which arises simply because a particle in the central region is farther than a correlation length away from both ends. The resulting distribution in $q_\perp$ is predicted to be a universal

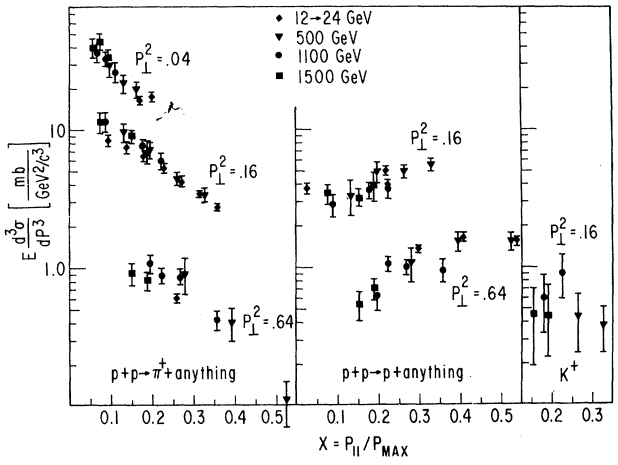

(a)

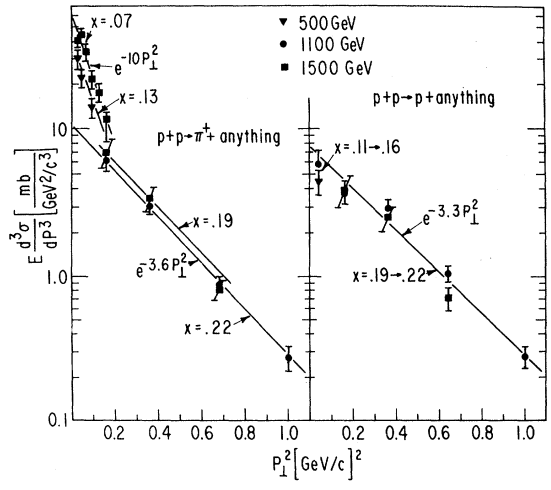

(b)

FIG. 2.10. Data on $pp \to c$+anything ($c=p$, π^+, K^+) from CERN intersecting storage rings (Krisch, 1971), with lower-energy data included for comparison (a) as a function of x, for fixed $p_\perp^2$, and (b) as a function of $p_\perp^2$, for fixed x. Energies shown are equivalent lab energies.

function, depending only on the type of particle produced.

2. *Speculations Concerning Asymptotic Energies*

At what energies should these asymptotic forms be valid? Assume for the purpose of speculation the existence of a universal correlation length L in the variable y. Then there are several distinct energy regions

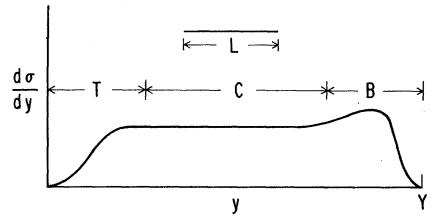

FIG. 2.11. Hypothetical single-particle inclusive spectrum as a function of rapidity. Illustrated are target fragmentation region T, central plateau C, and beam fragmentation region B, as well as correlation length L. (These designations are only qualitative; dimensions on the figure should not be taken literally.)

depending on the length $Y=\ln(s/\mu^2)$ of the rapidity plot. See Table 2.3 for a tabulation of Y vs s and E_{lab}.

Low-energy region, $Y \lesssim L$. In this region the y plot is shorter than one correlation length, so that the distribution is nowhere limiting.

Limiting fragmentation energy region, $Y \gg L$. As soon as the energy is such that $Y \gg L$, particles with y near one end of the spectrum decouple from the opposite end. Hence the distribution becomes limiting near the ends, and the limiting portion spreads as the energy increases.

Plateau energy region, $Y \gg 2L$. For $Y \gg 2L$, the entire distribution is expected to take its limiting form. Every value of y is now at a distance large compared L from at least one end. As Y becomes large compared to $2L$, the central plateau should develop. As Y increases further, the only expected change in the single-particle inclusive spectrum is that the central plateau lengthens. In this region the multiplicity should increase like $\ln(s)$.

Since $s=\mu^2 e^Y$, doubling Y means *squaring* s. That is, if s_F is the threshold of the limiting fragmentation region, and if s_p is the threshold of the plateau region, then we find $s_p \propto s_F^2$.

Which of these energy regions are reached by current experiments? The evidence on limiting distributions presented in Sec. II.C shows that the reaction $pp \to \pi X$ possesses a limiting fragmentation region, to within the 25%–30% experimental accuracy, at 13 GeV (see Fig. 2.9). It seems likely that many reactions have reached approximate limiting fragmentation at energies of 10–30 GeV, and perhaps even lower in some cases. See Lander's review (1971) for additional relevant data.

TABLE 2.3. Length $Y=\ln(s/\mu^2)$ of the rapidity plot for pions of transverse momentum $q_\perp=350$ MeV, for various values of c.m. total energy $s^{1/2}$ and E_{lab} in pp collisions.

Y	4	5	6	7	8	9	10
$s^{1/2}$ in GeV	2.8	4.6	7.6	12.5	20.6	34.0	57.4
E_{lab} in GeV	3.3	10.6	30.0	83	227	615	1750

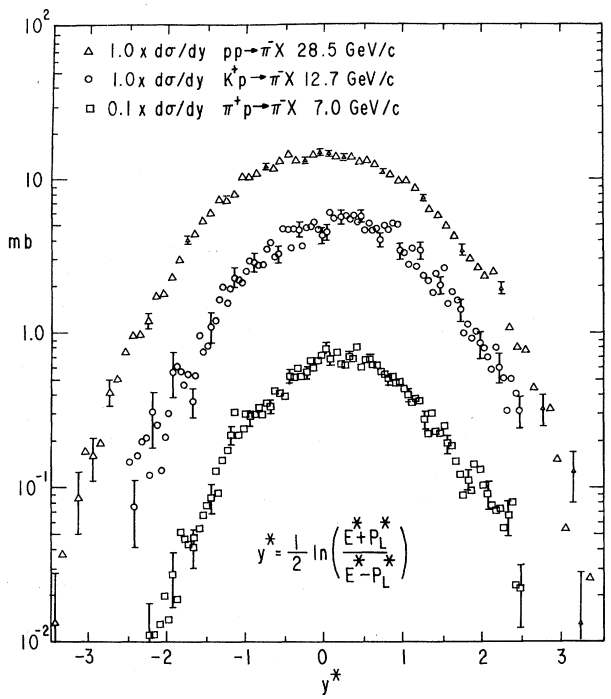

FIG. 2.12. Some experimental single-particle inclusive spectra, as functions of the CM rapidity. (BNL–Rochester–Wisconsin collaboration (Chen *et al.*); communicated by T. Ferbel and L. L. Wang at the Cal Tech conference "Phenomenology in Particle Physics, 1971".)

Theoretical arguments based on the Mueller approach presented in Sec. II.E (Abarbanel, 1971a) suggest a correlation length $L=(1-\alpha_M)^{-1}\approx 2$. Correlations due to prominent low-energy resonances also lead to an estimate of $L\approx 2$. If these estimates are correct, then the energy at which approximate limiting fragmentation would begin to be observed is $Y\gtrsim 3$–4, and a central plateau should begin to develop at $Y\gtrsim 6$–8. Table 2.3 gives the relation between Y and beam energy, for pions of $q_\perp=350$ MeV produced in pp collisions. Our estimates translate into fragmentation limits being approached at 2–4 GeV, and a plateau beginning to appear at 30–200 GeV.

Have any reactions begun to develop a central plateau in existing experiments? Some rapidity plots compiled by the BNL-Rochester-Wisconsin collaboration,[9] Chen *et al.*, are shown in Fig. 2.12. Although one can see increasing rounding at the higher energies, no real plateau is apparent. At ISR energies, one should see the plateau, if it exists. Unfortunately the data available at this time, shown in Fig. 2.10, do not extend into the central region. If the correlation length is $L\approx 2$, and we then ask for y more than two correlation lengths from the end of the plot, we need $|x|<0.02$! To dramatize the difference between the x and y variables, we show in Fig. 2.13 some of the data from Fig. 2.10, replotted as a function of y. We eagerly await the filling in of the central region!

[9] Private communication of unpublished data by L. L. Wang and T. Ferbel at the CalTech conference "Phenomenology in Particle Physics, 1971".

3. Central Plateau and Logarithmic Growth of Multiplicities

Existence of a central plateau implies that the average multiplicity of final-state particles must rise logarithmically with s. This can be seen from the normalization relation, Eq. (2.32), expressed in terms of y

$$\int dyd^2q_\perp \rho_{ab}{}^c(y, q_\perp, s)=\langle n_c\rangle, \tag{2.44}$$

where $\langle n_c\rangle$ is the average multiplicity of particles of type c. Performing the integral over transverse momenta, one can write

$$\sigma_{ab}{}^{-1}\int dy(d\sigma_{ab}{}^c/dy)=\langle n_c\rangle. \tag{2.45}$$

The integral over y in Eq. (2.45) gives two contributions to the multiplicity; a constant contribution coming from the fragmentation regions, and a contribution from the plateau region. The latter contribution grows logarithmically with energy, since the plateau length grows with Y. Explicitly, this plateau contribution to the multiplicity is given by

$$\langle n_c\rangle = B_c \ln s + \text{const},$$
$$B_c=(1/\sigma)(d\sigma^c/dy)\,|_{\text{plateau}}. \tag{2.46}$$

Thus the height of the plateau in y determines the coefficient of the logarithmic term in the multiplicity.

We are not yet able to use Eq. (2.46) without further assumptions, because we have no data which show a clear plateau. Bali, Brown, Peccei, and Pignotti (1970a) pointed out, however, that one can use this equation to test the speculation that medium-energy data around 30 GeV might be at the threshold for development of a central plateau. In this case, $(d\sigma/dy)_{\text{plateau}}$ would be equal to the maximum height of the distribution in Fig. 2.12, which is about 14 mb for $pp\to\pi^-X$ at 28.5 GeV/c. To compare with the Echo Lake data in Fig. 2.1, we must normalize to the inelastic cross section, since they measure the multiplicity in inelastic collisions only. Using $\sigma_{\text{inel}}\approx 33$ mb (see Holder *et al.*, 1971), we find $B_{\pi^-}\approx 0.42$. If we assume that the charged particles measured at Echo Lake consist of equal numbers of π^+ and π^- (ignoring a K correction of uncertain magnitude) we infer from Table 2.1 a value of B_{π^-} ranging from 0.36 to 0.48, depending on which fit is used. The theoretical value obtained from Eq. (2.46) using the speculation of onset of the plateau at 30 GeV is in agreement, within the considerable uncertainties.

These speculations may be roughly correct, but they are probably as oversimplified a picture as were the initial attempts to predict asymptotic behavior of two-body amplitudes using Regge poles. In Sec. II.E, we shall be able to say more about the approach to the limit. Detailed predictions must, however, employ

specific models. One such prediction using a multiperipheral model (Pignotti and Ripa, 1971) shows a rather slow approach to a plateau, with considerable curvature in the central region even at ISR energies.

4. Two-Particle Correlations

The short-range order hypothesis predicts the vanishing of two-particle correlations if the rapidities of the two particles differ by much more than a correlation length. We discuss this prediction briefly in this section, and defer further discussion of correlations to Sec. II.E.

Defining the two-particle inclusive density as in Eq. (2.30), we have

$$\rho_{ab}^{c_1c_2}(\mathbf{q}_1, \mathbf{q}_2; s) \equiv (E_1E_2/\sigma_{ab})[d\sigma(ab\to c_1c_2X)/d^3q_1d^3q_2]. \tag{2.47}$$

It is also useful to define a two-particle correlation function $C^{(2)}$,

$$C_{ab}^{c_1c_2}(\mathbf{q}_1, \mathbf{q}_2; s) = \rho_{ab}^{c_1c_2}(\mathbf{q}_1, \mathbf{q}_2; s) - \rho_{ab}^{c_1}(\mathbf{q}_1, s)\rho_{ab}^{c_2}(\mathbf{q}_2, s). \tag{2.48}$$

Then the short-range correlation hypothesis states that

$$C_{ab}^{c_1c_2}(y_1, \mathbf{q}_{1\perp}; y_2, \mathbf{q}_{2\perp}; s) \sim 0 \quad \text{for} \quad |y_2 - y_1| \gg L. \tag{2.49}$$

Consider, for example, the case where y_1 is in the target fragmentation region, and y_2 is in the beam fragmentation region, and $y_2 - y_1 \gg L$. Then using Eq. (2.41) and (2.42) one obtains the result

$$\rho_{ab}^{c_1c_2}(\mathbf{q}_1, \mathbf{q}_2; s) \cong \gamma_a^{c_1}(y_1, q_{1\perp})\gamma_b^{c_2}(Y - y_2, q_{2\perp}), \tag{2.50}$$

where the γ's are the same functions measured in single-particle spectra.

E. Mueller Analysis of Inclusive Reactions

1. Generalized Optical Theorem

A new method of analysis of inclusive reactions introduced by Mueller (1970) inspired by related work on

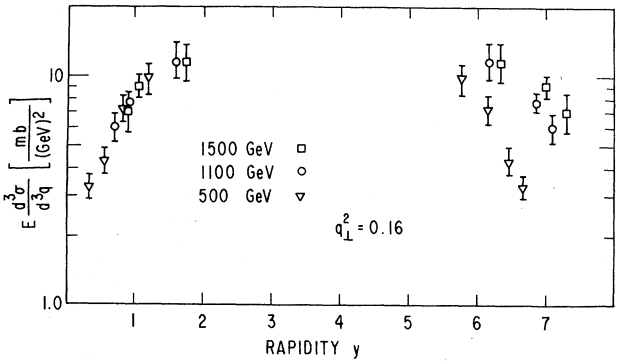

FIG. 2.13. A replotting of some of the ISR data from Fig. 2.10 as a function of rapidity.

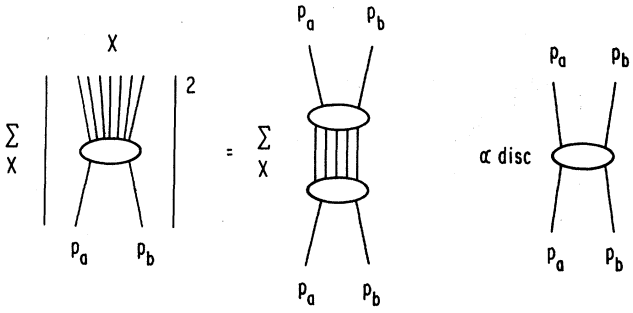

FIG. 2.14. Schematic display of unitarity relation between total cross section and imaginary part of forward scattering amplitude.

μ-pair production by Altarelli, Brandt, and Preparata (1971) is proving very useful in suggesting further theoretical and phenomenological developments. The first step in Mueller's analysis can be regarded as a generalization of the optical theorem. The optical theorem, based on unitarity, says that the cross section for $a+b\to$anything is equal (up to phase space factors) to the imaginary part (or absorptive part, or discontinuity in s) of the amplitude $a+b\to a+b$ in the forward direction. This is shown pictorially in Fig. 2.14. Similar relationships exist (DeTar, 1971a; Tan, 1971a; Stapp, 1971) between the n-particle inclusive reaction

$$a+b\to c_1+c_2+\cdots+c_n+X, \tag{2.51}$$

where X represents anything else produced, and the forward limit of a discontinuity in M^2, the missing mass,[10] of the amplitude for the process

$$a+b+\bar{c}_1+\bar{c}_2+\cdots+\bar{c}_n\to a+b+\bar{c}_1+\bar{c}_2\cdots+\bar{c}_n. \tag{2.52}$$

For simplicity we limit the discussion here to the single particle inclusive reaction

$$a+b\to c+X, \tag{2.53}$$

whose cross section turns out to be proportional to a discontinuity[10] of the forward amplitude

$$a+b+\bar{c}\to a+b+\bar{c}. \tag{2.54}$$

The relationship is shown pictorially in Fig. 2.15, in close analogy to the treatment of the optical theorem in Fig. 2.14. The relation between the inclusive cross section and the appropriate[10] absorption part $A(p_a, q, p_b)$ of the three-body amplitude is

$$E_q(d\sigma/d^3q) \equiv \rho(q_{\parallel}, q_\perp, s) = s^{-1}A(p_a, q, p_b), \tag{2.55}$$

where some irrelevant normalization constants have been absorbed in A.

[10] The correct discontinuity in M^2 is the one which is equal to the sum over intermediate states of the modulus squared of the production amplitude. For a precise specification see (Tan, 1971a).

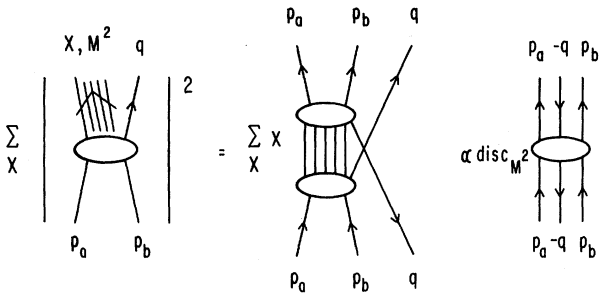

FIG. 2.15. Generalized unitarity relation for single-particle inclusive reactions, relating them to absorptive part of forward three-body amplitude.

It will be convenient to express A as a function of the invariants

$$s=(p_a+p_b)^2,$$

$$t=(p_b-q)^2,$$

$$u=(p_a-q)^2,$$

$$M^2=(p_a+p_b-q)^2. \tag{2.56}$$

These are related in the usual way

$$s+t+u=M^2, \tag{2.57}$$

where mass terms have been dropped in the high-energy limit.

The utility of these expressions becomes apparent only in the high-energy limit. Mueller proceeds to develop asymptotic expansions using Toller's method (Toller, 1965), a very elegant and systematic prescription for extracting asymptotic expressions. Rather than attempt to develop the Toller machinery here, we shall adopt a more heuristic approach. There are two limits to discuss, and we begin with the central, or pionization, region.

2. *Central Region*; *Double-Regge Limit*

In what we have called the central (or pionization) region; that is, the region in which $q_{||}{}^*$ is small in the cm system of p_a and p_b and in which the rapidity y is near the center of its allowed range, both t and u are large and comparable in magnitude. In this kinematic region it is easy to show [for example, by using Eqs. (2.65) and (2.67)] that

$$tu\cong\mu^2 s, \tag{2.58}$$

where $\mu^2=q_\perp{}^2+m^2$. This limit in which both t and u become large is appropriate to evaluation by a double-Regge expansion, indicated by the diagram of Fig. 2.16. Assuming that the leading contribution is given by Regge Poles (not branch points) one finds the result[11]

$$A(s,t,u)=l^{\alpha_l(0)}u^{\alpha_u(0)}\tilde{f}(q_\perp). \tag{2.59}$$

From Fig. 2.16 we see that both Regge poles carry vacuum quantum numbers, so that the leading behavior should be given by the Pomeron.[12] Then Eq. (2.59) simplifies to

$$\begin{aligned}A(s,t,u)&=(tu)^{\alpha_P(0)}\tilde{f}_{ab}{}^c(q_\perp)\\&=s^{\alpha_P(0)}f_{ab}{}^c(q_\perp),\end{aligned} \tag{2.60}$$

where Eq. (2.58) has been used in the final step, and where the subscripts have been added to the function $f_{ab}{}^c(q_\perp)$ to identify the incident particles, and the superscript c identifies the observed final-state particle.

Using Eq. (2.60) in Eq. (2.55) one finds

$$F_{ab}{}^c(q_{||},q_\perp,s)=s^{\alpha_P(0)-1}f_{ab}{}^c(q_\perp) \tag{2.61}$$

for the single-particle inclusive spectrum. If $\alpha_P(0)=1$, the distribution approaches a constant limit as $s\to\infty$. If $\alpha_P(0)$ should be slightly less than unity, the single-particle density, ρ, defined in Eq. (2.31) as the distribution F, divided by the total cross section σ_{ab} will still approach a constant as $s\to\infty$.

Another prediction of Eq. (2.60) is that in the central, double-Regge region the single-particle spectrum $f_{ab}{}^c(q_\perp)$ in independent of $q_{||}$ as well as of s. This is equivalent to the prediction of a central plateau in the rapidity variable y, which resulted from the short-range correlation model (see Sec. II.D.). If the leading singularities are Regge poles, factorization is expected, so that

$$f_{ab}{}^c(q_\perp)=\beta_a\beta_b\gamma^c(q_\perp), \tag{2.62}$$

where β_a is the Pomeron coupling to particle a, and where $\gamma^c(q_\perp)$ is now a universal function, depending only on the observed particle. Since the couplings β_a and β_b determine the magnitude of the total cross sec-

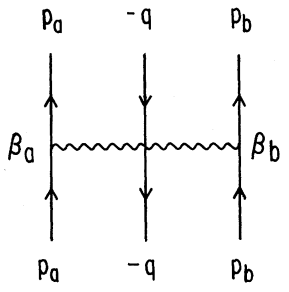

FIG. 2.16. Mueller diagram describing double-Regge limit appropriate to central plateau region of single-particle spectrum.

[11] This wobbly foundation underlines all the predictions which follow. Although the energy dependence would be modified by logarithms if branch points are important, this effect would be hard to detect. Factorization is easier to test, and should be tested as accurately as possible. It should be remembered, however, that whereas a breakdown of factorization implies non-pole terms, the converse is not true.

[12] That the Regge singularities which govern the asymptotic behavior of A are the same as those which govern the asymptotic behavior of two-body reactions is a plausible, but unproved, hypothesis.

tion σ_{ab}, one can write the universal relation

$$\rho_{ab}{}^{c}=E_q/\sigma_{ab}(d\sigma_{ab}{}^{c}/d^3q)=\gamma^c(q_\perp), \qquad (2.63)$$

independent of which particles a and b are incident. Remember, however, that this relation holds only for sufficiently high energies to permit both t and u to be large; see Sec. II.D.2 for further discussion of this point.

3. *Fragmentation Regions; Single-Regge Limit*

The limit $t\to-\infty$, u fixed, $s\to\infty$, and $q_\perp$ fixed is the target fragmentation region. To see this, go to the lab frame and use the parameterization used in defining the rapidity y in Sec. (II.B.3)

$$\begin{aligned} q&=(u\cosh y, q_x, q_y, \mu\sinh y),\\ p_a&=(m_a, 0, 0, 0),\\ p_b&=(m_b\cosh y_b, 0, 0, m_b\sinh y_b), \end{aligned} \qquad (2.64)$$

where $\mu^2=q_\perp{}^2+m^2$. Since s is large, $s\cong m_am_b\exp(y_b)$. From the definition of u it follows that

$$u=m_a{}^2+m^2-2\mu m_a\cosh y. \qquad (2.65)$$

Thus fixed u and fixed $q_\perp$ imply fixed y (and therefore fixed $q_{||}$ in the lab frame). The appropriate form of the Regge limit is then

$$E_q(d\sigma_{ab}{}^{c}/d^3q)=F_{ab}{}^{c}(q_{||}, q_\perp, s)\cong(t^{\alpha(0)}/s)\tilde{f}_{ab}{}^{c}(q_\perp, q_{||}) \qquad (2.66)$$

which is indicated diagrammatically in Fig. 2.17(a).

In the target fragmentation region t is proportional to s, as we can easily see by evaluating t in terms of y from Eq. (2.50),

$$t=m^2+m_b{}^2-2\mu m_b\cosh(y_b-y)\cong-(\mu e^{-y}/m_a)s \qquad (2.67)$$

Using Eq. (2.67) we can rewrite the single-Regge limit form, Eq. (2.66), as

$$F_{ab}{}^{c}(q_{||}, q_\perp, s)=s^{\alpha_P(0)-1}f_{ab}{}^{c}(q_\perp, q_{||})=f_{ab}{}^{c}(q_\perp, q_{||}), \qquad (2.68)$$

where we have again assumed Pomeron dominance, and assumed $\alpha_P(0)=1$.

From Fig. 2.17(a) we see that factorization implies that all the dependence on the beam particle is contained in a factor β_b, so that we can write

$$f_{ab}{}^{c}(q_\perp, q_{||})=\beta_b\tilde{\gamma}_a{}^{c}(q_\perp, q_{||}{}^{L}). \qquad (2.69)$$

Since Regge theory says that $\sigma_{ab}\cong\beta_a\beta_b$, one can divide by the total cross section to obtain a function which is independent of the nature of the beam:

$$\rho_{ab}{}^{c}=(1/\sigma_{ab})F_{ab}{}^{c}=\gamma_a{}^{c}(q_\perp, q_{||}). \qquad (2.70)$$

Similar results hold in the beam fragmentation region, where u is large and t fixed. According to Eq. (2.67), this corresponds to fixed $y-Y$, or fixed $q_{||}$ in the projectile rest frame (which we designate as $q_{||}{}^{b}$), and has the single-Regge limit shown in Fig. 2.17(b),

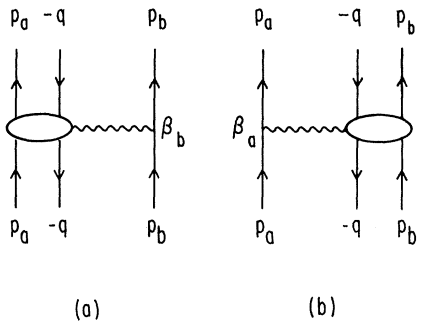

FIG. 2.17. Mueller diagrams describing single-Regge limit appropriate to fragmentation regions of single-particle spectrum. (a) Target fragmentation region, (b) Projectile fragmentation region.

which gives the result

$$F_{ab}(q_{||}, q_\perp, s)=s^{\alpha_P(0)-1}f_{ab}{}^{c}(q_\perp, q_{||}{}^{b}). \qquad (2.71)$$

Factorization then implies that

$$f_{ab}(q_\perp, q_{||}{}^{b})=\beta_a\tilde{\gamma}_b{}^{c}(q_\perp, q_{||}{}^{b}). \qquad (2.72)$$

Finally, one can divide by the total cross section to obtain the density which is independent of the nature of the target,

$$\rho_{ab}{}^{c}=\gamma_b{}^{c}(q_\perp, q_{||}{}^{b}). \qquad (2.73)$$

4. *Approach to Limit; Secondary Trajectories*

By including secondary trajectories in the Mueller analysis, one can discuss the rate of approach to the asymptotic limit (Chan, 1971a; Abarbanel, 1971a). For example, in the target fragmentation region, the inclusion of a secondary trajectory, α_M would give an expression

$$F_{ab}(q_{||}, q_\perp, s)=f_{ab}{}^{P}(q_\perp, q_{||})+s^{\alpha_M(0)-1}f_{ab}{}^{M}(q_\perp, q_{||}). \qquad (2.74)$$

Secondary trajectories can be isolated by taking differences of single-particle spectra; for example, the difference between π^+ and π^- on protons isolates the ρ. If $\rho^{\pm}(q_{||}, q_\perp, s)$ describes the target fragmentation spectra of the reactions

$$\pi^{\pm}+p\to c+X$$

then we have

$$\rho^{+}(q_{||}, q_\perp, s)-\rho^{-}(q_{||}, q_\perp, s)=2f^{\rho}(q_\perp, q_{||})^{\alpha_\rho(0)-1}. \qquad (2.75)$$

An interesting speculation is the extension of duality arguments to predict reactions which attain their limiting values at lower energies (Chan, 1971a). For example, $K^++p\to\pi^{\pm}+X$ is related in Mueller's analysis to the three-body reaction $K^++p+\pi^{\mp}\to K^++p+\pi^{\mp}$. This reaction has exotic quantum numbers in the $ab\bar{c}$ channel. By analogy to two-body reactions, Chan *et al.*

TABLE 2.4. Comparison of some predictions made by three different criteria which have been proposed concerning exotic channels and rapid approach to the fragmentation limit (Chan, 1971a; Ellis, 1971; Einhorn, 1971).

	Fragmentation limit attained at low energies?		
Reaction	Chan *et al.*	Ellis *et al.*	Einhorn *et al.*
$K^+p\to\pi^-X$	yes	yes	yes, p frag; no, K frag
$K^+p\to\pi^+X$	yes	yes	no
$\pi^+p\to\pi^-X$	yes	no	no
$pp\to\pi^\pm X$	yes	yes	no
$pp\to K^-X$	yes	yes	yes

conclude that the contributions of the secondary meson trajectories vanishes, $f^M=0$. Such reactions should then show limiting behavior at lower energies than nonexotic channels.

It seems, however, that the application of duality to the six-point function is not straightforward—several papers have appeared recently which criticize the Chan *et al.* criterion (Ellis, 1971; Chan, 1971b; Chen, 1971b; Einhorn, 1971; Kugler, 1971). Alternate criteria for the absence of secondary trajectories in the fragmentation limit have been proposed: Ellis *et al.* say that it is indeed necessary that $(ab\bar{c})$ be exotic, but sufficiency requires (ab) exotic also. Einhorn *et al.* say that necessary and sufficient criteria are (ab) exotic, plus $(b\bar{c})$ exotic in the target fragmentation region (our convention is that a is the target, b is the beam) or $(a\bar{c})$ exotic for beam fragmentation. Examples of reactions where the three criteria differ are given in Table 2.4. We know of no data which discriminate clearly among these tests. It should also be pointed out that finding energy variation where none is predicted clearly violates the prediction, whereas finding no energy variation where such variation is allowed could occasionally occur "accidentally."

The approach to the fragmentation limit described by Eq. (2.74) can also be expressed in terms of the correlation length picture described in Sec. II.D, by rewriting that equation in the form

$$F_{ab}(q_{\|},q_\perp,s)=f_{ab}{}^P(q_\perp,q_{\|}) + \exp(-Y/L)\mu^2 f_{ab}{}^M(q_\perp,q_{\|}), \quad (2.74a)$$

where

$$L=(1-\alpha_M(0))^{-1}\approx 2, \quad (2.74b)$$

thus exhibiting the prediction of the correlation length made by the Mueller–Regge picture.

The approach to the limit in the central region can similarly be treated by including secondary trajectories in the diagram of Fig. 2.16. The leading terms as $s\to\infty$ come from Pomeron exchange on one side and secondary trajectory (M) exchange on the other,

$$\rho_{ab}{}^c(q_{\|},q_\perp;s)\cong\gamma^c(q_\perp)+\exp[-(\tfrac{1}{2}Y-y^*)/L]\tilde{\gamma}_{PMb}{}^c(q_\perp) + \exp[-(\tfrac{1}{2}Y+y^*)/L]\tilde{\gamma}_{aMP}{}^c(q_\perp)\cong\gamma^c(q_\perp) + s^{-1/4}[\gamma_{PMb}{}^c(q_\perp)\exp(y^*/L)+\gamma_{aMb}{}^c(q_\perp) \times\exp(-y^*/L)]. \quad (2.76a)$$

Note that the approach to the central plateau is relatively slow; the secondary trajectory vanishes only as $s^{-1/4}$. If particle a is the same as particle b, as in $pp\to cX$, the secondary term simplifies to (Abarbanel, 1971a)

$$\rho_{ab}{}^c(q_{\|},q_\perp;s)\cong\gamma^c(q_\perp)+s^{-1/4}\gamma_{PM_P}{}^c(q_\perp)2\cosh(y^*/L). \quad (2.76b)$$

Not only the rate of approach to the limit, but also the shape of the secondary contribution is predicted.

The secondary term in Eq. (2.76) will contribute to the average multiplicity, via Eq. (2.32). If $\gamma_{PM_P}{}^c$ is positive, $\langle n\rangle$ will curve downward as a function of $\ln s$ to its eventual linear behavior, and the central region of the single-particle inclusive spectrum will show a depression in its center before the plateau limit is reached. If $\gamma_{PM_P}{}^c$ is negative, $\langle n\rangle$ will curve upward and the single-particle spectrum will have a hump in the middle.

5. *Experimental Test of Factorization*

One of the factorization predictions discussed above has already received a measure of experimental confirmation. In the target fragmentation region (the region of small laboratory momenta $q_{\|}$) the prediction of Eq. (2.70) is that the inclusive spectrum divided by the total cross section is independent of the beam momentum or beam particle type:

$$\rho_{ab}{}^c\cong\gamma_a{}^c(q_\perp,q_{\|}), \quad (2.77)$$

where γ_a depends on the fragment and or the type of target, but not on the beam. A Brookhaven–Rochester–Wisconsin collaboration (Chen, 1971a) has collected data on the following reactions,

$$\pi^+p\to\pi^-+X \text{ at } 7 \text{ GeV}/c, \quad (a)$$

$$K^+p\to\pi^-+X \text{ at } 12.7, \quad (b)$$

$$pp\to\pi^-+X \text{ at } 28.5, \quad (c)$$

$$\pi^-p\to\pi^-+X \text{ at } 24.8, \quad (d)$$

$$\pi^-p\to\pi^++X \text{ at } 24.8. \quad (e)$$

Since reactions (a)–(d) have the same target and same particle observed in the final state, they should obey Eq. (2.77), provided that the energies are high enough. Figure 2.18(a) shows the results of Chen *et al.* The agreement for reactions (a)–(c) is quite good, but reaction (d) agrees less well. It is interesting to note that this is just what Chan *et al.* (1971a) predict by regarding the first three reactions as exotic,

whereas (d) is nonexotic and therefore expected to approach its asymptotic limit more slowly. It will be very interesting to have more such data at a greater variety of energies.

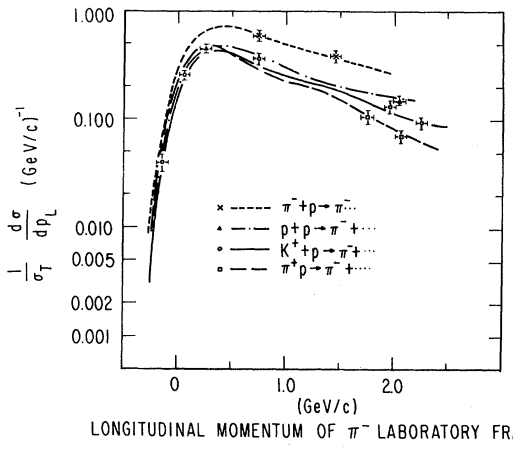

(a)

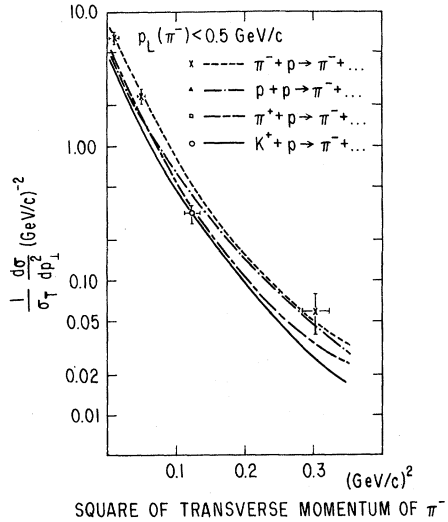

(b)

FIG. 2.18. Momentum distributions in the laboratory for four reactions at different energies (see text). Each reaction is normalized by its asymptotic total cross section. Equality of distributions tests factorization and hypothesis of limiting fragmentation (Chen, 1971a). (a) Longitudinal momentum distributions. (b) Transverse momentum distributions. Curves shown are fits to data. Typical points show size of errors.

In Fig. 2.18(b) the dependence on $q_\perp^2$ is shown for the region of $q_{||}<0.5$ GeV/c; again the spectra normalized by the total cross section agree quite well, especially the three exotic reactions at small $q_\perp^2$. Table 2.5 shows quantitatively how good the agreement is.

The BNL–Rochester-Wisconsin collaboration also analyzed the beam fragmentation region for $\pi^+p\to\pi^-X$ and $\pi^-p\to\pi^+X$. This is the region where $q_{||}$ in the projectile rest frame, $q_{||}{}^b$, is small. In this region the asymptotic amplitudes for Reactions (a) and (e) are represented by the two Mueller diagrams in Fig. 2.19. Since the Pomeron carries vacuum quantum numbers, these two diagrams and hence the two spectra should be equal asymptotically. In Fig. 2.20(a) the data of Chen *et al.* are shown, and the two reactions agree roughly in shape and magnitude—probably as well as could be expected in view of the large difference in incident energy.[13] In Fig. 2.20(b) the corresponding $q_\perp{}^2$ distributions are shown.

TABLE 2.5. The second column gives the single-particle inclusive cross section for $q_{||}<0.5$ GeV/c. The third column shows these cross sections divided by their asymptotic total cross sections.

Reaction	$\int_0^{0.5}\frac{d\sigma}{dq_{||}}dq_{||}$	$\sigma_{\text{tot}}{}^{-1}\int_0^{0.5}\frac{d\sigma}{dq_{||}}dq_{||}$
(a)	5.3±0.4 mb	0.23±0.02
(b)	3.5±0.4 mb	0.20±0.02
(c)	9.1±0.6 mb	0.23±0.02
(d)	7.9±0.6 mb	0.32±0.02

6. *Phase Space Boundary; Triple-Regge Limit*

In those portions of the fragmentation regions which are near the phase space boundary, $x\approx\pm1$, more specific predictions can be made about single-particle inclusive spectra. Consider the limit $s\to\infty$, $t=(q-p_b)^2$ fixed, and for the moment, $M^2=(p_a+p_b-q)^2$ fixed also. An ordinary Regge limit is appropriate here,

$$d\sigma/dtdM^2=(1/s^2)\beta(t,M^2)(s/M^2)^{2\alpha(t)}. \quad (2.78)$$

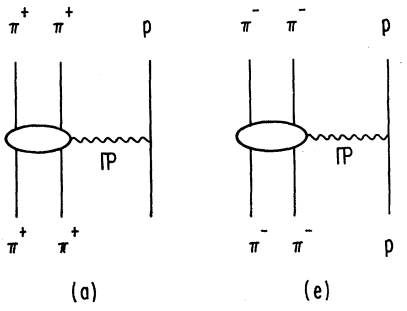

FIG. 2.19. Mueller diagrams for reactions (a) $\pi^+p\to\pi^-X$ and (e) $\pi^-p\to\pi^+X$.

[13] From Fig. 2.21 one can infer that the difference between the two reactions should come from ρ exchange. We know from two-body Regge phenomenology that the $pp\rho$ vertex is small at $t=0$, since it is predominantly spin-flip. Hence the ρ contribution should be suppressed, and the difference between $\pi^+p\to\pi^-X$ and $\pi^-p\to\pi^+X$ in the beam fragmentation region should be small.

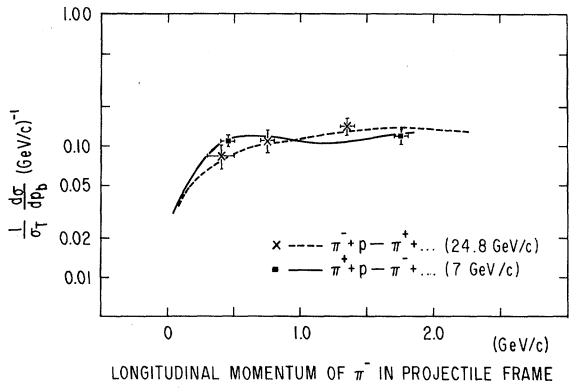

(a)

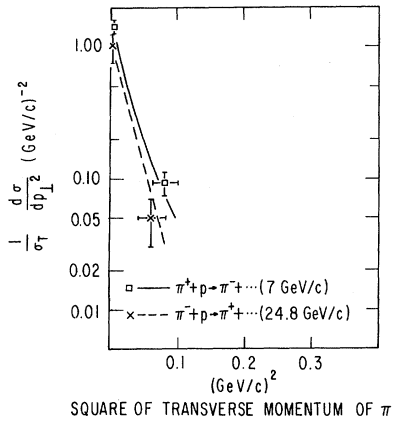

(b)

FIG. 2.20. Momentum distributions in the projectile rest frame of $\pi^+p\to\pi^-X$ at 7 GeV/c, and $\pi^-p\to\pi^+X$ at 24.8 GeV/c. (a) Longitudinal momentum distributions, (b) transverse momentum distributions (Chen, 1971a).

Now let M^2 become large also, but keep s/M^2 large enough that the Regge limit taken above is still valid. From Fig. 2.21, one sees that $\beta(M^2, t)$ can be interpreted as a Reggeon-particle total cross section, which should be proportional to $(M^2)^{\alpha_v(0)}$, where $\alpha_v(0)$ denotes a Regge trajectory with vacuum quantum numbers. The cross section then becomes

$$d\sigma/dtdM^2=(1/s^2)\gamma(t, M^2)(s/M^2)^{2\alpha(t)}(M^2)^{\alpha_v(0)}. \quad (2.79)$$

To pin down the M dependence of $\gamma(t, M^2)$ let us translate Eq. (2.79) from the variables t, M^2 to x, $q_\perp$ (Elitzur, 1971). Fixed t as $s\to\infty$ implies that we are in the beam fragmentation region, where Table 2.1 tells us that

$$M^2/s\approx 1-x. \quad (2.80)$$

Use of this relation and the fact that

$$dq^3/E_q=\pi dM^2dt/s \quad (2.81)$$

allows us to rewrite Eq. (2.79) in the form

$$E_q(d\sigma/dq^3)=F(x, q_\perp, s)$$
$$\cong\alpha(t, M^2)(1-x)^{\alpha_v(0)-2\alpha(t)}s^{\alpha_v(0)-1}. \quad (2.82)$$

Now t is a function of x and $q_\perp$ in this region, so $F(x, q_\perp, s)$ will scale if $\alpha_v(0)=1$, and if $\gamma(t, M^2)$ is independent of M^2. Imposing these conditions we finally obtain

$$F(x, q_\perp)\cong\gamma(t)(1-x)^{1-2\alpha(t)}, \quad (2.83)$$

where

$$\gamma(t)=(16\pi)^{-1}\,|\,\beta_{bP}(t)\,|^2\beta_{aP}(0)g_{RRP}(t). \quad (2.84)$$

The β's are the usual Regge couplings, normalized according to the prescription of Abarbanel *et al.* (1971c). The factor $g_{RRP}(t)$ is a Reggeon–Reggeon–Pomeron coupling (see Fig. 2.21).[14] At the other boundary, $x\approx -1$, a similar formula can be obtained,

$$F(x, q_\perp)\cong\gamma(u)(1+x)^{1-2\alpha(u)}. \quad (2.86)$$

Interesting and encouraging applications of the triple-Regge formula have already been made with medium-energy data (Chliapnikov, 1971; Peccei, 1971; Ting, 1971; Wang, 1971), although these energies are insufficient to allow both M^2 and s/M^2 to be comfortably large.

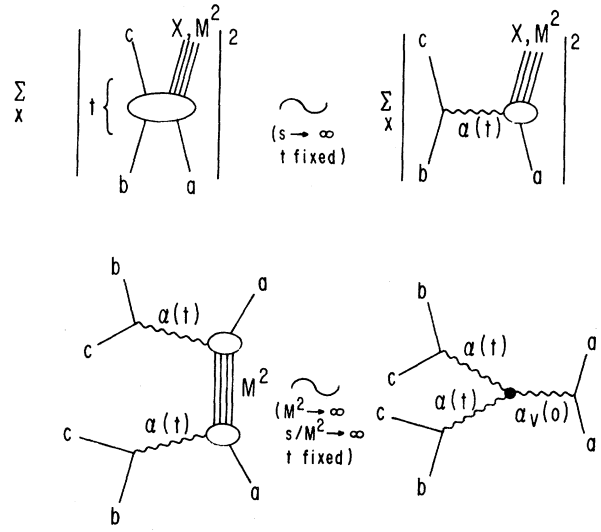

FIG. 2.21. Triple-Regge limit, $s\to\infty$, $s/M^2\to\infty$, t fixed. Wavy lines represent Regge roles.

[14] Equation (2.83) has a long history which the interested reader can find recounted in footnote 5 of Peccei (1971). It has been derived by the Mueller approach (DeTar, 1971c), from the multiperipheral model (Caneschi, 1969b; Silverman, 1970b) and by Feynman (1969). Chou and Yang (1970) arrived at a qualitative version of the result from a fragmentation picture, but Chou's quantitative version (Chou, 1971) disagrees with Eq. (2.83) in having a power one unit higher. We do not find Chou's intuitive arguments as convincing as those which arrive at Eq. (2.83).

Great theoretical interest is currently focussed on the case in which the Reggeons are pomerons, which may be observable in diffraction dissociation into high missing mass. For additional discussion of the triple-Pomeron coupling see Sec. III.A.

7. *Two-particle Inclusive Spectra; Correlations*

The Mueller approach relates two-particle inclusive spectra in $ab\to cdX$ to a discontinuity in M^2 of the forward scattering amplitude $ab\bar{c}\bar{d}\to ab\bar{c}\bar{d}$. One can then make Regge expansions appropriate to the various regions of the kinematical variables. We shall consider only the configuration available at medium energies, where the rapidity y_c is in the target fragmentation region, and y_d is in the beam fragmentation region. The appropriate Mueller diagram is shown in Fig. 2.22. The asymptotic limit, given by Pomeron exchange, is just the product of single-particle spectra

$$\rho_{ab}{}^{cd}(\mathbf{q}_c\mathbf{q}_d;\, s)\cong\gamma_a{}^c(y_c,\, q_{c\perp})\gamma_b{}^d(Y-y_d;\, q_{d\perp}). \quad (2.87)$$

The correlation function $C_{ab}{}^{cd}$, defined in Eq. (2.48) as the difference between the two-particle spectrum and the product of the single-particle spectra, vanishes in this limit.

The rate of approach to the limit will again be given by secondary trajectories, and the simplest possibility is of the form

$$C_{ab}{}^{cd}(\mathbf{q}_c,\, \mathbf{q}_d;\, s)\cong \exp[-(y_d-y_c)/L]$$
$$\times\gamma_{aM}{}^c(y_c,\, q_{c\perp})\gamma_{bM}{}^c(Y-y_d,\, q_{d\perp}). \quad (2.88)$$

In order to test the exponential dependence without mixing in variation from the single-particle spectra, one must let y_d-y_c grow while keeping y_c and $Y-y_d$ fixed (that is, q_c and $q_d{}^b$ fixed). This can be done only by increasing s; tests of the vanishing of two-particle correlations in the fragmentation regions cannot be done cleanly at fixed energy. The situation is simpler when one or both particles are in the central region; see (Abarbanel, 1971a) for details.

The above treatment of correlations is, however, not completely general, even in the Mueller–Regge framework. Freedman, Jones, Low, and Young (1971) have used the Toller machinery to expand the forward eight-point function in a way which exploits the full $O(3, 1)$ symmetry of the forward amplitude. They find that the exchange of Toller–Regge poles with Toller quantum number M can induce *long-range* correlations of the form $\cos M\varphi$, where $\cos\varphi=\hat{q}_{c\perp}\cdot\hat{q}_{d\perp}$. Two-body Regge phenomenology favors $M=0$ for all high-ranking Regge poles, but branch points may introduce $M\neq 0$ contributions. At any rate, such tests for long-range correlations will be very interesting.

Additional correlation tests are possible with a polarized beam or target, and these can also be analyzed with the help of the Toller M quantum number. (Abarbanel, 1971a, e).

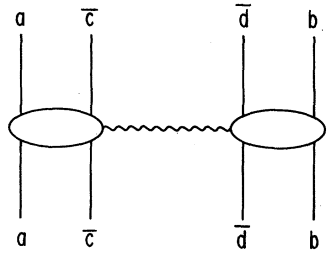

FIG. 2.22. Mueller diagram for two-particle inclusive spectrum when particle c is in the target fragmentation region, and particle d is in the beam fragmentation region.

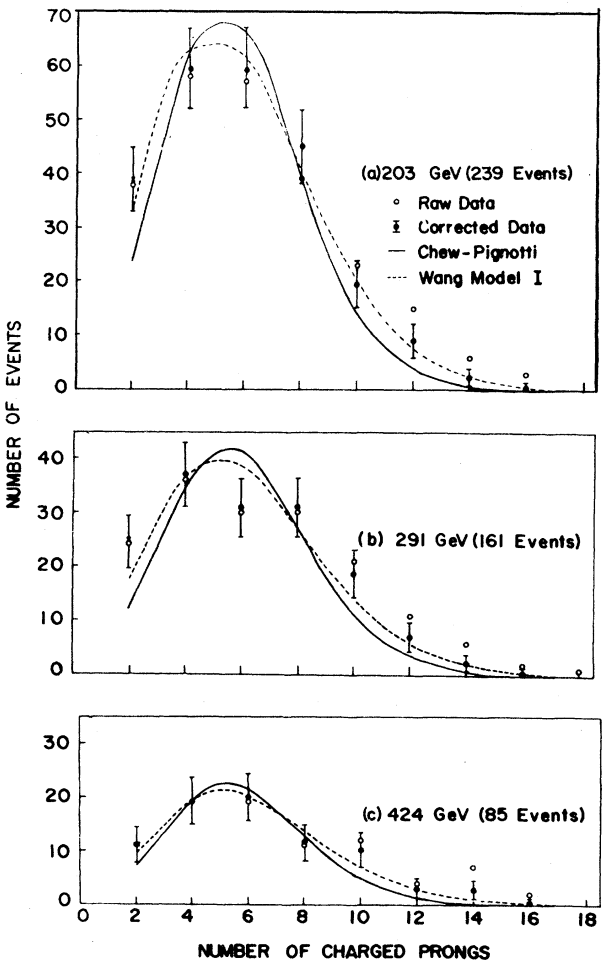

FIG. 2.23. Charged multiplicity distributions in Echo Lake cosmic ray data (Jones, 1970), with two Poisson-distribution fits.

F. Partial Cross Sections and Multiplicity Distributions

Another important class of data on multiparticle reactions is the observation of the number of particles produced. Since the neutrals are usually not observed, the data collected are numbers of events as a function of the number of charged prongs n_{ch} and as a function of beam energy. The resulting two-dimensional distribu-

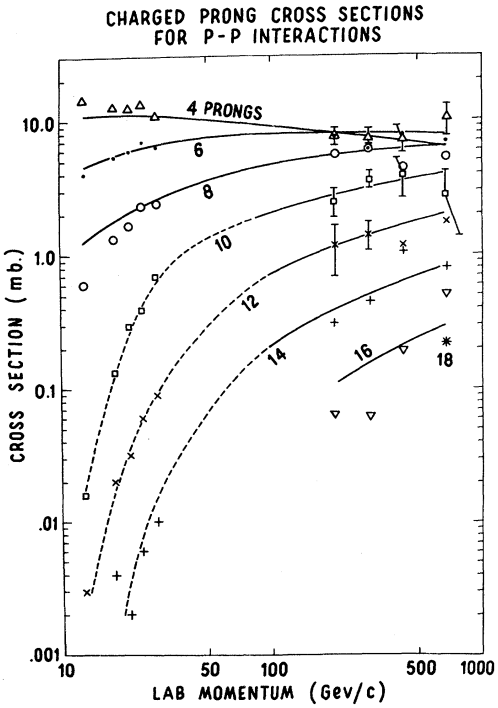

(a)

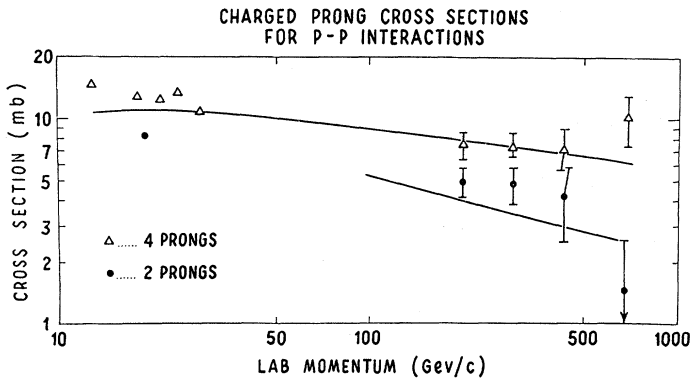

(b)

FIG. 2.24. Partial cross sections for $pp \to n$ charged prongs, Echo Lake and accelerator data (Lyon, 1971), with multiperipheral model fit (a) Four to 18 prong cross sections, (b) Two and four prong cross sections.

tion, $\sigma(n_c, E)$ properly normalized, is called a *charged-prong* cross section (or a *topological* cross section). The most extensive information on $\sigma(n_c, E)$ at high energies comes from the Echo Lake hydrogen-target cosmic-ray experiment (Jones, 1970; Lyon, 1970, 1971a). The multiplicity distribution, $\sigma(n_{ch}, E)$ as a function of n_{ch} at fixed E, is shown in Fig. 2.23; the charged prong cross section, $\sigma(n_{ch}, E)$ as a function of E for fixed n_{ch}, is shown in Fig. 2.24. The average charged multiplicity in inelastic events[15] $\langle n_{ch}(E)\rangle$ is shown in Fig. 2.1.

These pioneering data place important constraints on the model-builders. The data on $\langle n_{ch}(E)\rangle$ in Fig. 2.1, which are well fit by growth linear in $\ln E$, are uncomfortable to advocates of models which imply constant or power-law behavior. An example of the former is what we shall call the naive diffractive-fragmentation picture; an example of the latter is the Cheng-Wu iterated tower-diagram model (see Sec. III.C.). Verification of the apparent logarithmic growth of multiplicities would constitute a triumph for multiperipheral models—in fact, the prediction was contained in the classic Amati, Fubini, Stanghellini paper (1962). Nevertheless, other models based on quite different physical pictures can be made compatible with logarithmic growth; as we saw in Sec. II.D.3, any model with a nonvanishing central plateau will give logarithmic growth at sufficiently large s.

[15] Elastic events, $pp \to pp$, are excluded from these data, Figs. 2.23, 2.24, and 2.1.

The detailed two-dimensional distribution in Fig. 2.23 and 2.24 will impose much more severe constraints, but their present accuracy is insufficient to do this. For example, a definitive prediction of the diffractive picture is that individual partial cross sections approach constant limits at high energies. The plots of $\sigma(n_{ch}, E)$ for each n_{ch} shown in Fig. 2.24 are not inconsistent with this interpretation. On the other hand, the multiperipheral model predicts that each partial cross section σ_n rises to a maximum, then falls off with energy. This also is not inconsistent with Fig. 2.24, especially Fig. 2.24b. The solid lines are a fit based on the simplest multiperipheral model, the Chew-Pignotti model (1968), which predicts a Poisson form,

$$\sigma_n = c(\langle n\rangle^n e^{-\langle n\rangle}/n!). \tag{2.89}$$

The fit actually given by the solid lines in Figs. 2.23 and 2.24 follows a suggestion by C. P. Wang (1969a) that one use a Poisson distribution in *pairs* of produced charged particles; the parameters used are (see Lyon, 1970; and Table 2.1)

$$\langle n\rangle = \tfrac{1}{2}(\langle n_c\rangle - 2), \tag{2.90a}$$

where

$$\langle n_c\rangle = A + B \ln Q \qquad Q = s^{1/2} - 2m_p. \tag{2.90b}$$

Again, the point here is not so much the detailed fit, as the observation that the present data do not dis-

tinguish between the constant diffractive prediction and the multiperipheral-type fit.

The multiplicity distribution, $\sigma(n_{ch}, E)$ at fixed E, is often fit with a Poisson-type distribution. Examples shown in Fig. 2.23 give a fairly good fit to the data. Any model in which particles are produced in uncorrelated clusters (including some multiperipheral models) will give rise to a Poisson distribution in multiplicity of clusters. Assumptions about the nature of the clusters give a degree of freedom in data fitting. More general multiperipheral models, which allow finite-range correlations (see Sec. II.D), do not necessarily yield simple Poisson distributions. This is illustrated in a particular model by Ball and Marchesini (1970), and discussed in general by Mueller (1971).

The data can also accommodate totally different multiplicity distributions. As Hwa (1971) has pointed out, it is possible to have $\langle n\rangle$ growing logarithmically with energy even in a diffractive picture where $\sigma(n, E)\cong\sigma(n)$, independent of energy, if the multiplicity distribution is

$$\sigma(n)\propto n^{-2}. \tag{2.81}$$

In this case, the sum $\sum n\sigma(n)$ would diverge logarithmically, except that there is an upper limit imposed by the available energy $s^{1/2}$, with the result that the multiplicity grows as $\ln s$. The distribution in Eq. (2.81) is compatible within the errors with the tails of the distributions in Fig. 2.23. It is, however, very different from the Poisson distribution for $n\gg\langle n\rangle$, and more accurate data on high-multiplicity events will easily discriminate between the two distributions.

III. MODELS OF MULTIPARTICLE REACTIONS

In this section we discuss specific models of multiparticle reactions in somewhat more detail than the general remarks of Sec. II, although the presentation is still necessarily very sketchy. The models chosen are those which seem to us to be having the greatest influence, either on the organization of current data or on further theoretical development. Some models which have been of considerable historical importance are therefore not included. Moreover, the distinction between a model and a set of ideas about or a picture of multiparticle reactions is an arbitrary one. Some very influential ideas (for example, Feynman's ideas about high-energy reactions) are scattered through various sections, rather than being gathered together under the heading of a single model.

A. Multiperipheral Models

We shall discuss in this section a class of models, loosely described as "multiperipheral", which are in some general ways consistent with present experimental evidence concerning multiparticle production (Amati, 1962; Fubini, 1964; Kibble, 1963; Ter-Martirosyan, 1963). They have played a significant role in correctly predicting experimental behaviors, such as scaling for the single particle spectrum and the existence of pionization, and have provided a framework for the bootstrap models of Regge poles. General features predicted by multiperipheral models independent of the details which distinguish them, but resulting from the basic topological structure common to all of them, were discussed in Sec. II.D. under the heading "Short-range correlation hypothesis." In this section we discuss multiperipheral models more specifically.

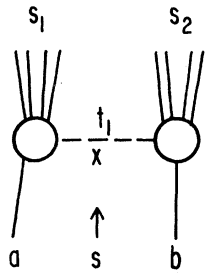

FIG. 3.1. Peripheral process, $a+b\to(s_1)+(s_2)$ with exchange of x. The kinematics are specified by s, t_1, and the invariant masses-squared, s_1 and s_2.

1. Definition

The multiperipheral idea has its origins in the singly peripheral description of high energy scattering. This description of a reaction is meaningful when

$$t_1^{\min}\approx(s_1s_2/s)<\tau \tag{3.1}$$

where τ is some peripheral range of momentum transfer, and s_1 and s_2 are the subenergies of the two blobs in Fig. 3.1. By singly peripheral, we mean that the full amplitude can be written as a product of the $a+x\to s_1$ amplitude and the $\bar{x}+b\to s_2$ amplitude times some propagator for the exchanged virtual particle x. Now, once this description becomes acceptable, a further decomposition of the amplitude can be performed as long as the kinematics allow it to be meaningful. If the total energy s is large, s_2 can be large enough so that it also admits a singly peripheral description (see Fig. 3.2). The criterion now is

$$t_2^{\min}\approx(s_2's_3/s_2) \tag{3.2}$$

be small. Continuing to N blobs, this gives

$$(s_1s_2\cdots s_N/s\tau^{N-1})\lesssim 1, \tag{3.3a}$$

where τ is some mean interblob momentum transfer. It is hard to reject this line of reasoning, once the singly peripheral description is accepted, unless one abandons the tacit assumption that the amplitude $b+\bar{x}\to s_2$ behaves essentially like an ordinary scattering amplitude. If x is a physical particle, such as a pion, this is hard to abandon, but if x is a Pomeron, many lines of speculation are open. For example, Hwa (1971), Silverman, Ting, and Yesian (1971), and Zachariasen (1971a) have speculated that a Pomeron can only be exchanged once, thus making the $P+b\to s_2$ reaction very different from an ordinary scattering amplitude.

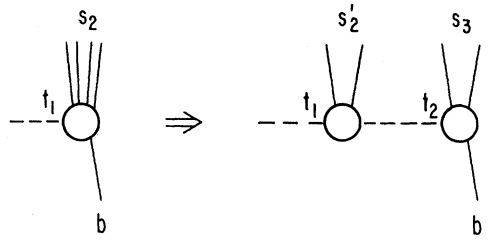

FIG. 3.2. Extension of peripheral to multiperipheral process.

Equation (3.3a) provides a simple, rough derivation of the law of logarithmic growth of multiplicities. Taking all the s_i equal to some average blob mass-squared s_0, one can rewrite Eq. (3.3a) as

$$N \lesssim c \ln (s/\tau), \tag{3.3b}$$

where $c^{-1} = \ln s_0/\tau$, and where N is the number of blobs. If each blob decays into n_b particles, logarithmic growth of $n = Nn_b$ results.

We have in this analysis used several ideas which are defining ingredients of all multiperipheral models.

(a) The momentum transfer dependence between successive links in the chain is damped rapidly. This restriction is necessary in order to limit the transverse momentum, $q_\perp$, of the produced secondary particles. Multiperipheral phase space is a very small segment of that allowed on purely kinematical grounds.

(b) Factorizability, or the property that the full amplitude can be written as a product of factors describing the dynamics in "local" regions of the multiperipheral chain. This property allows one to construct the matrix element for $n+1$—particle production by simply adding an additional link (factor) to the matrix element for n-particle production. Together with unitarity, and the approximate factorizability of phase space, this feature has been exploited to yield integral equations for the elastic scattering amplitude (Amati, 1962; Bertocchi, 1962; Chew, 1969a, b; Halliday, 1969a, b). These will be discussed in more detail below. Furthermore, we have seen in Sec. II.D. that the provision for only "nearest neighbor" interactions along the multiperipheral chain has far reaching consequences for the single particle spectrum and other inclusive experiments.

Various multiperipheral models for the n-particle production amplitude have been studied. Many of these are based on the assumed dominance of multipion exchange due to the proximity of the pion pole to the physical region, and the consequent enhancement for small momentum transfers. They are shown in Fig. 3.3 where the exchanged pions scatter to produce secondary pions with amplitude $T_{\pi\pi}$. Several models for the dynamics of $T_{\pi\pi}$ are the following:

(i) Dominance by low-energy resonances (Amati, 1962).

(ii) Inclusion also of a high-energy "tail" represented by Pomeron exchange (Chew, 1970a, b).

(iii) The use of duality to replace the low-energy direct-channel resonances of (i) by the exchange of lower-lying Regge trajectories (P', ρ) in the crossed channel, in addition to the Pomeron exchange of (ii) (Ball, 1969a, b).

Other multiperipheral models which have been proposed are multi-Regge exchange models (Kibble, 1963; Ter-Martirosyan, 1963; Bali, 1967; Zachariasen, 1967a, b) which have their origin in the Regge description of two-body scattering at high energies. This description may be valid when all the subenergies $s_{ij} = (q_i + q_i)^2$, between outgoing neighboring particles are large, as indicated by some experimental analyses (Chan, 1967; Lipes, 1969). However, much of the available multiperipheral phase space, as well as observed events, occur at small subenergies $\sim$1 GeV^2. In order to use a Regge description in this low-energy region, one must rely very heavily on duality (Chew, 1968a)—namely that the asymptotic Regge form is valid in an average sense, in the low energy resonance region.

All of the models so far discussed satisfy the basic criteria of multiperipheralism as stated above. They describe multiparticle production in terms of a linear chain of repeating links. The actual details of the links differ from model to model, but we shall see below that many general predictions follow independent of these details. In the following section we shall explore the consequences of a simple model for multiparticle production to illustrate how their general features come about.

2. *Chew-Pignotti Model*

We now examine in more detail a multiperipheral model based on some of the physical principles that have been previously discussed. We have already noted that since all the transverse momenta are limited, the real degree of freedom in multiparticle production processes lies in the longitudinal motion. DeTar (1971), exploits this empirical fact by simply ignoring the transverse momentum degrees of freedom and formulates the Chew-Pignotti model (Chew, 1968b) in only one dimension. This involves the simplification of uncoupling the transverse momenta in the Regge behavior of the particle subenergies by the approximation $(s_{ij})^{\alpha(t)} \approx$

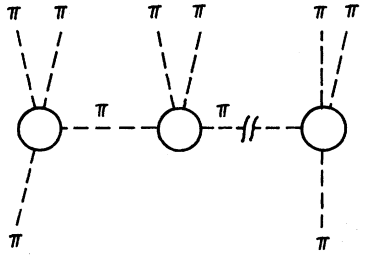

FIG. 3.3. Amati-Fubini - Stanghellini multiperipheral model.

s_{ij}^{α}, where α is some effective value of the trajectory. By means of this approximation, he illustrates in a straightforward manner the general features of the cross sections and single-particle distributions which follow from any multiperipheral mechanism for particle production.

The process we consider is

$$a+b\to 0+1+\cdots+n+(n+1), \tag{3.4}$$

that is, there are $n+2$ particles in the final state. In the laboratory system, where particle a is at rest and particle b moves along the z direction, we specify the momenta of the outgoing particles in terms of the rapidity variable discussed in Sec. II.B.3

$$\begin{aligned} p_a &= (m_a, 0, 0, 0), \\ p_b &= (m_b \cosh y_b, 0, 0, m_b \sinh y_b), \\ q_i &= (\mu_i \cosh y_i, \mathbf{q}_{i\perp}, \mu_i \sinh y_i), \end{aligned} \tag{3.5}$$

where $\mu_i^2 = q_{\perp i}^2 + m_i^2$. For large energies, $s=(p_a+p_b)^2$ is exponentially related to y_b

$$s = m_a^2 + m_b^2 + 2m_a m_b \cosh y_b \cong m_a m_b e^{y_b}. \tag{3.6a}$$

Moreover, if $y_j \gg y_i$, it follows that

$$s_{ij} = (q_i+q_j)^2 \cong \mu_i \mu_j \exp(y_j - y_i). \tag{3.7}$$

The differential element of phase space for n-particle production is

$$d\phi_n = \prod_{i=0}^{n+1} \frac{d^3 q_i}{E_i} \delta^4\Big(\sum_{i=0}^{n+1} q_i - q_a - q_b\Big) \tag{3.8}$$

which can be cast in terms of our new variables using the combinations $q_0+q_{\|}$ and $q_0-q_{\|}$

$$\begin{aligned} d\phi_n = \tfrac{1}{2} \prod_{i=0}^{n+1} d^2\mathbf{q}_{\perp i}\, dy_i\, \delta^2\Big(\sum_{i=0}^{n+1} \mathbf{q}_{\perp i}\Big) \\ \times \delta\Big[\sum_{i=0}^{n+1} \mu_i \exp(-y_i) - m_a - m_b \exp(-y_b)\Big] \\ \times \delta\Big[\sum_{i=0}^{n+1} \mu_i \exp(y_i) - m_a - m_b \exp(y_b)\Big]. \end{aligned} \tag{3.9}$$

The n-particle production cross section is (ignoring irrelevant constant factors that do not depend on n)

$$\sigma_n \propto \exp(-y_b) \int g^{2n} \prod_{i=0}^{n} (s_{i,i+1})^{2\alpha}\, d\phi_n, \tag{3.10}$$

where the integrand is the square of a multi-Regge matrix element and g is the coupling constant at the Reggeon–Reggeon-particle vertex, α is an "effective" Regge trajectory (since we are ignoring momentum transfers) and $\exp(-y_b)$ is the usual flux factor s^{-1} in our normalization. One of the assumptions of the model is that all the subenergies, $s_{i,i+1}$, are large. In this kinematical domain, usually referred to as the "strong ordering" limit, (Zachariasen, 1967) we have

$$E_{i+1} \gg E_i \gg \mu_i \tag{3.11}$$

and the delta functions in the phase space may be approximated by[16]

$$\frac{\exp(-y_b)}{m_a m_b} \delta(y_0 - x_a)\delta(y_b - y_{n+1} - x_b), \tag{3.12}$$

where $x_a = \ln(\mu_0/m_a)$ and $x_b = \ln(\mu_{n+1}/m_b)$. Furthermore, in this limit, we find, using Eq. (3.6), the relation

$$s \cong s_{01} s_{12} \cdots s_{nn+1} / (\mu_1^2 \mu_2^2 \cdots \mu_n^2) \tag{3.13}$$

so that we may write

$$\begin{aligned} \sigma_n &\propto \exp(-y_b) g^{2n} \exp[y_b(2\alpha-1)] \int \prod_{i=1}^{n+1} dy_i \delta(y_b - y_{n+1}) \\ &\propto \exp(-y_b) g^{2n} \exp[y_b(2\alpha-1)] \\ &\quad \times \int^{(y_b)} dy_n \int^{y_n} dy_{n-1} \cdots \int^{y_2} dy_1 \\ &\propto g^{2n} \exp[y_b(2\alpha-2)] \frac{(y_b)^n}{n!} \propto s^{2\alpha-2} \frac{(g^2 \ln s)^n}{n!}, \end{aligned} \tag{3.14}$$

where in the spirit of ignoring the transverse momenta, we have assumed $\mu_i = m_i$ and taken for simplicity $m_0 = m_a$, $m_{n+1} = m_b$. The total cross section is simply

$$\sigma_T = \sum_{n=0}^{\infty} \sigma_n \propto s^{2\alpha-2+g^2}. \tag{3.15}$$

Thus Regge behavior emerges in a multiperipheral model. In order to obtain constant (or nearly constant) total cross sections one requires

$$2\alpha - 2 + g^2 = 0. \tag{3.16}$$

Using this relation one finds, from Eq. (3.14), the result

$$\begin{aligned} \sigma_n &= c s^{2\alpha-2} [(g^2 \ln s)^n / n!] \\ &= c[(g^2 \ln s)^n \exp(-g^2 \ln s)/n!], \end{aligned} \tag{3.17}$$

which is simply a Poisson distribution with an average multiplicity which grows logarithmically with energy,

$$\bar{n} = g^2 \ln s. \tag{3.18}$$

(See Sec. II.F for a more general discussion and comparison of these results with experiments.)

Efforts to make the Chew–Pignotti model more realistic of course destroy the simplicity of the result in Eq. (3.17). See, for example, Ball and Marchesini (1969a, b) and Chew, Rogers, and Snider (1970). But the model, although obviously oversimplified, exhibits most of the general, successful predictions of multiperipheral models.

Now we calculate the prediction of this model for the single particle distribution function as measured in inclusive experiments. For the n-particle production process we can calculate the probability that the ith particle in the chain has momentum $q_{\|i} = \mu_i \sinh y$ by

[16] Note the extremity of this assumption: It says that the leading particle carries away practically all the energy.

inserting a delta function $\delta(y-y_i)$ in Eq. (3.14)

$$\frac{d\sigma_{n,i}(y, y_b)}{dy} \propto \exp[y_b(2\alpha-2)]g^{2n} \times \int \prod_{j=1}^{n+1} dy_j \delta(y_b-y_{n+1})\delta(y-y_i)$$

$$\propto \exp[y_b(2\alpha-2)]g^{2n} \frac{y^{i-1}}{(i-1)!} \frac{(y_b-y)^{n-i}}{(n-i)!}. \quad (3.19)$$

Since we cannot distinguish an observed particle's position in the multiperipheral chain, the spectrum for producing a single particle in conjunction with $n-1$ others is obtained by summing over i

$$\frac{d\sigma_n(y, y_b)}{dy} = \sum_{i=1}^{n} \frac{d\sigma_{n,i}(y, y_b)}{dy} \propto \exp[y_b(2\alpha-2)]g^{2n} \frac{Y^{n-1}}{(n-1)!}, \quad (3.20)$$

where we see that the distribution is flat, independent of y. The total "inclusive" spectrum, where no distinction is made in the number of produced particles is obtained by summing over n,

$$d\sigma(y, y_b)/dy = \sum_n [d\sigma_n(y, y_b)/dy] \propto \exp[y_b(2\alpha-2+g^2)] \quad (3.21)$$

which is also flat in y and has the same asymptotic behavior as the total cross section Eq. (3.15).

The simple physical picture which emerges from this analysis is that the produced particles are on the average uniformly spaced in y, with a density proportional to g^2. Consequently as the energy increases, the physical region opens up linearly with y_b; or equivalently, Y, and the mean multiplicity grows as $g^2 \ln s$.

More general investigations based on the multiperipheral model confirm the simple picture given by the Chew–Pignotti model. The property of scaling (Feynman, 1969) or the existence of a limiting distribution (Benecke, 1969) for the inclusive single particle spectrum (see Sec. II.C) has been shown to be a property of all multiperipheral models (Silverman, 1971b) that have so far been proposed. This is due to the damping in momentum transfer, factorization, and to the generation of the Pomeranchuk Regge singularity in these models. In the multiperipheral model, the exponential damping of the single particle spectrum in $q_\perp^2$ has been shown to follow from an assumed exponential damping in momentum transfer of the residue of the exchanged Regge trajectories (Bali, 1971; Silverman, 1971c).

The phenomenon of pionization, that is, the existence of slow particles in the center of mass system, was first shown to exist in the pion exchange multiperipheral model by Amati, Fubini, and Stanghellini (1962). Their proof was directly extended to show the existence of pionization for multi-Regge exchange models (Silverman, 1971b) as well. In the multiperipheral model, the pionization property can be described either by a continuous, non-zero limit of the single particle distribution at $x \to 0$ in the center of mass system, or by a flat plateau in the rapidity variable (see Sec. II.D, where these properties are discussed more fully).

3. *Multiperipheral Bootstrap Models*

The simple Chew–Pignotti model discussed in the previous section illustrates the possibility of constructing multi-Regge bootstrap models. The behavior of the total cross section calculated from the model is that of a Regge pole with intercept α_{out}, where

$$\alpha_{\text{out}} = 2\alpha_{\text{in}} - 1 + g^2, \quad (3.22)$$

where α_{in} is the input Regge trajectory. The equality is illustrated schematically in Fig. 3.4.

Some important features of multiperipheral bootstraps can be seen from Eq. (3.22):

(a) The constant g^2 controls the multiplicity. Comparing Eq. (3.18) and Eq. (2.1), and estimating that one-third of the particles produced are neutrals, one estimates $g^2 \approx 1.3$. Since $\alpha_{\text{out}} \approx 1$, it follows from Eq. (3.22) that $\alpha_{\text{in}} \approx .35$. This is consistent with the interpretation of α_{in} as an average over secondary mesonic trajectories (P', ρ, π, etc). It is inconsistent with multiple Pomeron exchange being a dominant contribution.

(b) Multiple exchange of a Pomeron with intercept unity, $\alpha_{\text{in}}=1$, gives $\alpha_{\text{out}}=1+g^2$, in violation of the Froissart bound. This Finkelstein-Kajantie (1968) effect is quite general. Either one sets $g_P^2=0$ (Gribov, 1967), or $\alpha_P(0)<1$. The latter option, chosen by Chew and Pignotti, gives total cross sections which fall with energy as $s^{-\epsilon}$, where ϵ can probably be taken small enough not to violate existing data.

Chew, Goldberger, and Low (1969a) put the multi-Regge bootstrap into the form of an integral equation, and many authors have worked on their equations in the meantime (see, for example, the review of Frazer, 1970). A generalized partial-wave projection of the equations can be made which allows one to investigate the J-plane singularities of the scattering amplitude. We shall not go into detail, but merely mention some relatively recent interesting results:

(a) Complex Regge poles emerge from such equations (Ball, 1969a, b; Chew, 1970b); their phenomeno-

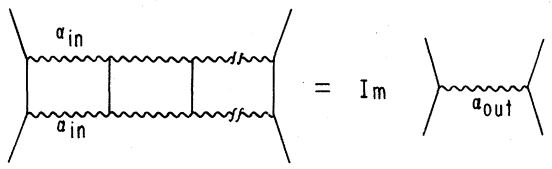

FIG. 3.4. Symbolic version of multiperipheral bootstrap equation.

logical implications are now being explored (Zachariasen, 1971). They can give rise to polarizations, and even to wiggles in total cross sections.

(b) Realistic models usually fail to give a Pomeron with sufficiently high intercept. Chew and Snider (1970a, 1971), in response to this difficulty, invented the "schizophrenic Pomeron", in which the P and P' are manifestations of fundamentally the same trajectory on different sheets of the complex J plane.

(c) The nature of the Pomeranchuk singularity, which we have called "the Pomeron" in this review, is an open question. A review by Zachariasen (1971a) examines many possibilities. It is universally agreed that it is not a simple Regge pole, but it is not known how good the pole approximation might be for phenomenological purposes. Much of the Mueller analysis in Sec. II.E relies on this simplifying assumption.

(d) The small parameter ϵ measuring the rate of decrease of total cross sections, $\sigma \propto s^{-\epsilon}$, implies in multiperipheral schemes the weakness of some internal Pomeron coupling. Abarbanel, Chew, Goldberger, and Saunders (1971c, d) identify the coupling as a "triple-Pomeron" coupling, which measures the strength of diffraction dissociation into high-mass states (see Sec. II.E.6).

We close this very brief review with the apology that this is not intended to be primarily a theoretical paper. We have therefore confined our remarks to those which might be of use in interpretation of data in the near future.

B. Diffractive Fragmentation Model

Yang and collaborators have developed a picture of high-energy hadronic reactions as the interpenetration of two spatially extended objects (Wu, 1965; Byers, 1966; Chou, 1968; Benecke, 1969; Chou, 1970). Although the subject of this review is multiparticle reactions, we must briefly review two-body reactions because the diffractive (or *droplet*) model had its origins there.

The picture of two hadrons, extended semitransparent objects with many degrees of freedom, passing through each other is made quantitative by an eikonal treatment. This treatment establishes a finite limit for $d\sigma/dt$ as $s\to\infty$, and provides a relation between this asymptotic limit and the hadronic matter density in the following way:

If the scattering amplitude $a(k)$ is defined by $d\sigma/dt=\pi a^2$, the eikonal approximation consists of writing

$$a(\mathbf{k})=\int [1-S(b)]\exp(i\mathbf{b}\cdot\mathbf{k})d^2\mathbf{b} \qquad (3.23)$$

where $\mathbf{k}$ is the two-dimensional momentum transfer, and $\mathbf{b}$ is the impact parameter in the plane transverse to the incoming beam:

$$\mathbf{k}=(k_x, k_y); \qquad k^2=-t$$
$$\mathbf{b}=(b_x, b_y).$$

Here $S(b)$ is the transmission coefficient (or the S matrix for a given impact parameter). The assumption underlying this formulation is that the wavelength of the incoming particle be small compared to the dimensions of any change in the transmitting medium. The quantity $-\log S(b)$ is called the opaqueness at the impact parameter b, in analogy to the scattering of a wave through a slab. Pursuing the analogy, one may write

$$-\log S(b)=K\iint D_A(\mathbf{b}-\mathbf{b}')D_B(\mathbf{b}')d^2\mathbf{b}', \qquad (3.24)$$

where

$$D(x, y)=\int_{-\infty}^{\infty}\rho(x, y, z)\,dz,$$

and ρ is the spherically symmetric matter density inside a hadron. K is some constant absorption coefficient. Equations (3.23) and (3.24) relate the scattering amplitude to the hadronic density. For pp elastic scattering, Chou and Yang (1968) identify the hadronic density with the charge density inside the protons. Using experimental fits to high-energy pp elastic scattering, they were able to predict the charge form factor $F_1(k^2)$ over a wide range of the momentum transfer.

Bearing in mind the droplet interpretation of high energy elastic scattering, Benecke *et al.* (1969) make the following argument for limiting fragmentation. As the energy increases, the projectile undergoes increasing Lorentz contraction as seen by the target. Constancy of σ_{el}, σ_{tot}, and $d\sigma/dt\,|_{\text{el}}$ at asymptotic energies suggest that the momentum and quantum number transfer process between the matter in the projectile and that in the target do not appreciably change when the projectile is further compressed. Thus one expects that excitation and subsequent breakup of the target would also approach a limiting distribution: Hence the limiting distributions $\rho^{(1)}(\mathbf{p})$, $\rho^{(2)}(\mathbf{p}_1, \mathbf{p}_2)$, etc. Empirical support for the existence of limiting single particle distributions is discussed in Sec. II.C.

Several qualitative predictions emerge from the diffractive fragmentation model: Rapid decrease of elastic cross sections for large t is a consequence of the idea that it is hard to keep a hadron intact when given too much transverse momentum (Wu, 1965). Consistent with this idea it is expected that in ep and hadron–hadron scattering, the partial cross sections $\sigma(M^*, t)$ should fall sharply with increasing momentum transfer t, when M^*, the invariant mass of the fragments, corresponds to the case of an elastic scattering or to the production of a resonance. For values of M^* in between the resonances and beyond the resonance region, the falloff in t should be more gentle. Experiments on deep inelastic electron scattering (Panofsky, 1968) seem to have this feature, but Bloom and Gilman (1970) have advanced an alternate interpretation in which there is no significant difference in the behavior of the resonances and the continuum. In pp scattering, however, there is a qualitative agreement with the

prediction mentioned above (Anderson, 1966; Amaldi, 1971).

Another consequence of a diffractive view of fragmentation is that all the partial cross sections σ_n, become constant at high energies. There is some evidence at rather low energies that partial cross sections for low multiplicities, i.e., small n, continue to persist in diffractive processes like $pp \to pp^*$ where p^* is a low-lying resonance with the quantum numbers of the proton (Cocconi, 1961; Anderson, 1966; Foley, 1967). The ratio μ^+/μ^- at sea level (Fuji, 1969; Appleton, 1971) remains approximately 1.25 from 3–100 Bev. This has been cited by Chou and Yang (1971) as support for the diffractive picture, but the constancy of the μ^+/μ^- ratio follows from scaling and the power-law behavior of the cosmic ray primary spectrum alone, and hence is obtained in all currently popular models (Frazer, 1971c).

We close this section with a discussion on multiplicity and pionization. If there are final state particles with finite momenta in the cm frame as $s \to \infty$, the phenomenon is termed "pionization" by some authors.[17] In terms of the scaled variable $x = 2p_{||}{}^{CM}/s^{1/2}$, this implies that the single-particle distribution $\rho(x, p_\perp)$ will approach a finite limit as $x \to 0$. In terms of the rapidity variable y, this corresponds to the prediction of a plateau in the center of the plot for $d\sigma/dy$ vs y. At first sight, the diffractive fragmentation model seems to exclude such a possibility as it envisages a hadron collision as that of two extended, semitransparent objects "going through" each other without arresting each other in the cm frame. Consider, however, the average multiplicity, given by

$$\langle n \rangle = \sigma_T{}^{-1}[\int \rho^T(\mathbf{p})(d^3p/E_p) + \int \rho^P(\mathbf{p})(d^3p/E_p)], \quad (3.25)$$

where $\rho^T(\mathbf{p})$ is the single-particle spectrum for the target fragments, and $\rho^P(\mathbf{p})$ is that of the projectile fragments.[18] In a diffractive fragmentation model where the fragments have finite momenta in the rest frame of the fragmenting particle, the integrals are convergent and the average multiplicity asymptotically becomes a constant. Should the multiplicity continue to increase with the incoming energy, the integrals of $\rho(\mathbf{p})$ must diverge. This implies that as $E \to \infty$, there are target fragments with infinite lab momenta.

If $\rho(\mathbf{q}) \cong$ const, for large $q_{||}$, one recovers $\langle n \rangle \propto \ln s$. Since $dq_{||}/E_q = dy$, this implies a uniform distribution on the y plot. Thus, logarithmically increasing multiplicities can be made consistent with a diffraction fragmentation picture. Such a single-particle spectrum may then be difficult to distinguish from that predicted by the multiperipheral model. In such a model, however, there is no reason why the factorization or short-range correlation predictions of Secs. II.D and E should hold.

A detailed model of the diffractive fragmentation type which incorporates growth of multiplicities like $\ln s$ has been constructed by Hwa (1971). See Sec. II.F for further discussion of multiplicities in diffractive and multiperipheral models.

C. Field Theory Models[19]

Regge's analysis of the asymptotic behavior of scattering amplitudes in potential theory led to insights which still dominate our attempts to understand high-energy hadronic processes. Very soon after the recognition of the importance of these insights, theorists turned to quantum field theory, to see if its high-energy limit would support the insights drawn from potential theory, and to see if it would lead to further insights applicable to high-energy processes. The intensity of this effort has increased in the past few years, led by the program of Cheng and Wu.[20]

Cheng and Wu have concentrated on the analysis of quantum electrodynamics with massive photons. Although this theory includes complications of spin and gauge invariance which can be avoided by looking at simpler theories (such as φ^3, which we shall discuss later), it is especially interesting because quantum electrodynamics is the only really reliable theory we have. Moreover, its spin structure leads to asymptotic behavior resembling that of diffraction scattering, even in the weak-coupling approximation on which all currently used techniques rely.

Although the techniques used by Cheng and Wu and the many others who have contributed to this field are of great theoretical interest, we confine our review to a discussion of results which may be relevant to high-energy hadronic processes. Various authors have used various methods (see Chang, 1968, for example), but all use the procedure of summing the leading terms as $s \to \infty$ in each order of perturbation theory. The fact that this procedure involves summing infinite sets of diagrams should not delude us into forgetting that it is still a weak-coupling approximation. To see this clearly consider as an example an amplitude of Regge form, depending on a parameter λ

$$T(\lambda) = \gamma(\lambda) s^{\alpha(\lambda)}, \quad (3.26)$$

where

$$\gamma(\lambda) = \sum_0^\infty \gamma_i \lambda^i \quad \text{and} \quad \alpha(\lambda) = \sum_0^\infty \alpha_i \lambda^i.$$

Expanding the factor $s^{\alpha(\lambda)}$, we have

$$T(\lambda) = s^{\alpha_0}(\sum_0^\infty \gamma_i \lambda^i)[1 + (\sum_1^\infty \alpha_i \lambda^i) \ln s + \tfrac{1}{2}(\sum_1^\infty \alpha_i \lambda^i)^2 \ln^2 s + \cdots] \quad (3.27)$$

[17] Chou and Yang define the term differently. To avoid confusion, it seems best to avoid this term.

[18] Note that our invariant normalization differs by a factor $1/E_q$ from that of Yang and collaborators.

[19] This section was heavily influenced by a review of F. Zachariasen (1971) and by conversation with R. L. Sugar and B. W. Lee.

[20] Among the multitude of Cheng-Wu references, a recommended starting point is Phys. Rev. Letters **24**, 1456 (1970). Other references can be found there.

Taking only the leading power of $\ln s$ in each order of λ, one finds

$$T(\lambda)=\gamma_0 s^{\alpha_0}[1+\lambda\alpha_1 \ln s+\tfrac{1}{2}(\lambda\alpha_1 \ln s)^2+\cdots]=\gamma_0 s^{\alpha_0+\alpha_1\lambda}, \tag{3.28}$$

a result which is zeroth order in λ for the residue function, and first order for the trajectory function.

In simpler field theories the leading log terms correspond to a sum of ladder graphs; in electrodynamics the gauge condition forces one to include some crossed graphs—the ladder is generalized to what is called a *tower*, shown in Fig. 3.5. The scattering amplitude which results from summing single-tower diagrams, $T_1(s, t)$, is of the form

$$T_1(s, t)=is\,[s^a/(\ln s)^2]F(t), \tag{3.29}$$

where $a=11\,\alpha^2\pi/32$, independent of t. The presence of the $(\ln s)^{-2}$ factor indicates that the complex j-plane singularity giving rise to this behavior is a fixed branch point, not a simple pole (in contrast to the φ^3 theory).

The most striking feature of this single-tower amplitude is that it gives a total cross section which rises as s^a, violating the Froissart bound. Therefore it cannot be the correct high-energy limit of the theory. The systematic procedure of summing the leading log terms in each order of perturbation theory has broken down, and what follows has more the status of a model—the sum of an arbitrarily-chosen set of diagrams. The set chosen is an s-channel iteration of t-channel towers, a reasonable choice to restore unitarity. This set, shown in Fig. 3.6 gives rise to a scattering amplitude with a simple eikonal form,

$$T(s, t)=s\int d^2\mathbf{b}\exp(i\mathbf{b}\cdot\mathbf{k})\,\frac{\eta(s, b)-1}{2i}, \tag{3.30}$$

$$=s\int d^2\mathbf{b}\exp(i\mathbf{b}\cdot\mathbf{k})\,\frac{\exp[\ln\eta(s, b)]-1}{2i}, \tag{3.31}$$

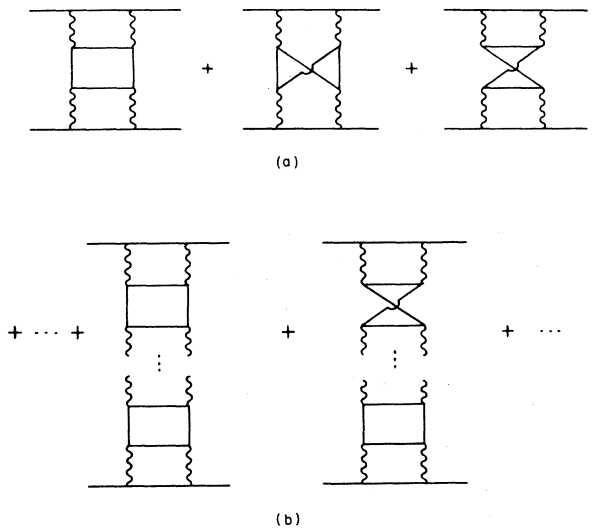

FIG. 3.5. Single-tower graphs (Cheng, 1970).

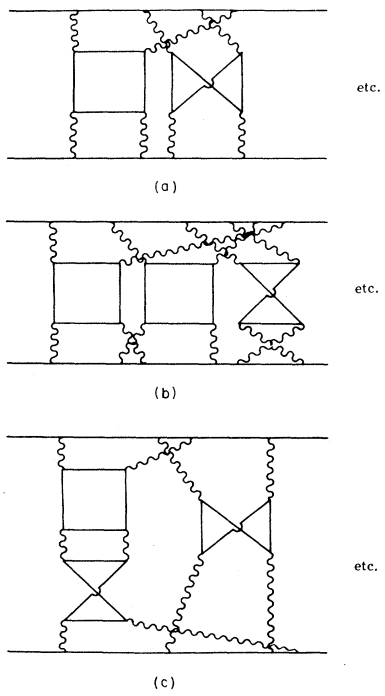

FIG. 3.6. Multi-tower graphs (Cheng, 1970).

where $\mathbf{k}^2=-t$, and where $T_1(s, t)$ is given by the lowest-order term in the expansion of $\exp[\ln\eta(s, b)]$

$$T_1(s, t)=-\tfrac{1}{2}(is)\int d^2\mathbf{b}\exp(i\mathbf{b}\cdot\mathbf{k})\ln\eta(s, b). \tag{3.32}$$

The emergence of the simple eikonal form in the context of relativistic quantum theory is one of the striking features of this and other closely related calculations (Abarbanel, 1969; Levy, 1969, 1970; Chang, 1970, 1971; Hasslacher, 1970; Cicuta, 1971; Muzinich, 1971; Tiktopoulos, 1971). The eikonal form, with the lowest-order term given by a simple Reggle pole, has had considerable success in data fitting (Arnold, 1967; Frautschi, 1969).

The novel feature of the present result is that the lowest-order term in the expansion of the exponential, the single-tower term, violates the Froissart bound, but is brought into conformity with unitarity in the final eikonal expression. The predictions of this eikonal amplitude are very interesting. According to Cheng and Wu, the single-tower amplitude corresponds to

$$\ln\eta(s, b)\propto-[s^a/(\ln s)^2]\exp(-b/b_0), \tag{3.33}$$

where b_0 is a constant. For s sufficiently large, this gives $\eta=0$, or complete absorption, for b less than a radius $R(s)$. For $b>R(s)$, η goes rapidly to unity, $\eta-1=0$, and there is no scattering. The physical picture is one of a black disc of radius $R(s)$.

Estimating $R(s)$ by taking it to be that value of b for which $\ln\eta=-1$, we find

$$R(s)\approx b_0\ln[s^a/(\ln s)^2], \tag{3.34}$$

or, for sufficiently large s,

$$R(s)\sim \ln s. \tag{3.35}$$

The picture is that of a black disk having a radius which grows as $\ln s$, in contrast both to the classical droplet or diffractive model, and to the Regge pole model, which corresponds to an increasingly transparent disk with radius growing as $(\ln s)^{1/2}$. The total cross section is then

$$\sigma_T(s)=4\pi\int_0^R b\,db=2\pi R^2\sim\left[\ln\frac{s^a}{(\ln s)^2}\right]^2 \tag{3.36}$$

and at sufficiently large s,

$$\sigma_T(s)\sim(\ln s)^2. \tag{3.37}$$

Another prediction is that since the amplitude is completely absorptive, $\sigma_{el}/\sigma_T=1/2$. Moreover, the amplitude has the usual black-disk diffractive form for sufficiently large s, so that it has zeros at $t=-(\beta_i/R)^2$, where the β_i are the zeros of J_1.

None of these predictions fit very well to observations at existing energies, especially the rising cross sections and the ratio of elastic to total cross sections. It is true, however, that some of the limiting forms we have used such as the passage from Eq. (3.34) to (3.35), are not valid at present energies, and the predictions of this model may be applicable at much higher energies.

Similar results have been found in φ^3 theory by Chang and Yan (1970), and by Hasslacher, Sinclair, Cicuta, and Sugar (1970). One important difference is that the single-tower amplitude is proportional to $s^{\alpha(t)}$, where $\alpha(t)=-1+g^2f(t)$. The limit -1 is characteristic of spinless particles. Thus whether or not the Froissart limit is violated by the single tower depends on the size of g^2. In this model the g^2 required to violate the bound is so large that the weak-coupling approximation is no longer valid.

Chang and Yan (1970) also look at production processes. They find that the model predicts pionization (the existence of the central plateau in y, or the dx/x behavior of the x-distribution), as one expects from a ladder-type model. The distribution is, however, multiplied by a factor s^a, so that scaling is not strictly true, and multiplicities rise as s^a. These latter predictions may be viewed with skepticism, because the eikonal form enforces the unitarity bound only on the elastic amplitude. A more sophisticated scheme, which included absorption in multiparticle states, might squelch the s^a growth.

In summary, it is a matter of taste as to how likely it is that these results carry over into the real world of high-energy hadronic processes. As we already remarked, the approximations used are weak-coupling approximations, and we are applying them to strong-coupling hadronic processes. Moreover, the field theory calculations assume elementary particles [the result $\alpha(0)>1$ in QED is a consequence of this], whereas hadrons are generally believed to be composite. The results are, however, quite striking, especially the rising cross section which results when the single-tower amplitude (which violates the Froissart bound) is tamed into the eikonal form. It provides us with a new family of models to use, should the higher-energy data require them.

D. Statistical Thermodynamical Model

The statistical model originally proposed by Fermi (1950), and refined and developed by Hagedorn and collaborators (Hagedorn, 1970a, b; Ranft, 1970) is difficult to integrate with the rest of the material of this review. The areas in which it is most successful are literally orthogonal to those on which we have concentrated. Whereas we have concentrated on longitudinal momentum distributions, the statistical model is the only model which predicts transverse momentum distributions.[21] Moreover, it predicts the particle density spectrum and relates the parameters of this spectrum to those of the transverse momentum distribution.

Statistical model of the particle spectrum. Hagedorn's statistical model of the particle spectrum (Hagedorn, 1967) is in one sense the most naive bootstrap model possible (there is no dynamics, only phase space), and in another sense the most complete (all possible intermediate states are included). Hagedorn states the bootstrap postulate in a particularly colorful way:

> A fireball is
> →a statistical equilibrium (hadronic black body radiation) of an undetermined number of all kinds of fireballs, each of which in turn is considered to be—,

where "fireball" is a particle or resonance. Frautschi (1971) has reduced this to more prosaic terms. The density of hadronic levels $\rho(m)$ is estimated from the number of states in a box, and is also required to be consistent with the spectrum of constituents, which are assumed to be the hadrons themselves. Self-consistent solutions exist of the form

$$\rho(m)=cm^a\exp(m/T_0), \tag{3.38}$$

where c is arbitrary; Frautschi finds $a<-5/2$, and Hagedorn finds $a=-5/2$.

Such a form is roughly consistent with the low-energy portion of the particle spectrum, as can be seen in Fig. 3.7 (Hagedorn, 1967), provided that T_0 is chosen to be about 160 MeV. Moreover, spectra of this form have also been derived from dual models and from models based on the Veneziano representation (Krzywicki, 1969a; Fubini, 1969a,b; Bardakci, 1969; Olesen, 1970a,b; Huang, 1970). The constant T_0 can be interpreted as the maximum possible temperature of ha-

[21] Recently a dual-model calculation in the Mueller approach has found an exponential cut-off for large $q_\perp^2$ (DeTar, 1971b).

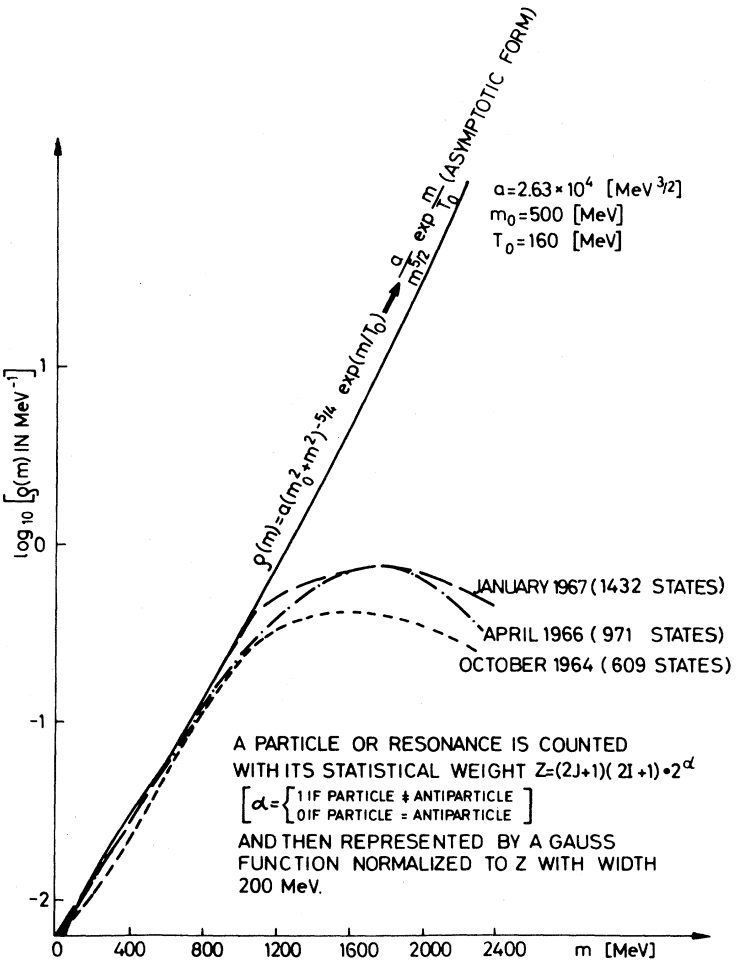

FIG. 3.7. Density of particle and resonance states, compared to statistical model prediction (Hagedorn, 1967).

dronic matter in equilibrium, since the average energy $\bar{E}$

$$\bar{E}=\int_0^\infty dm\, m\rho(m)e^{-m/T}\Big/\int_0^\infty dm\,\rho(m)e^{-m/T} \quad (3.39)$$

becomes infinite for $T>T_0$. Physically what happens is that as the energy is increased it goes into the creation of massive particles rather than into raising the kinetic energy of existing particles. Interesting astrophysical speculations have been made about the effect of a maximum temperature (Hagedorn, 1970c; Huang, 1970).

Transverse momentum distributions. The distribution of transverse momenta of secondaries produced in high-energy collisions follows rather directly from the statistical model, with a minimum of further assumptions. It is controlled by a statistical factor $\exp[-(q_{\|}{}^2+q_{\perp}{}^2+m^2)^{1/2}/T]$. The determination of T is model dependent, but at any rate T is not very much less than T_0 for high-energy collisions. One of the most impressive successes of the model is that transverse momentum distributions can be fit with the same value $T_0\approx160$ MeV determined from the particle spectrum in Fig. 3.7. Figure 3.8 from Hagedorn (1968) shows a comparison of calculated values of $\langle q_{\perp}\rangle$ with values inferred from cosmic ray data.

Production of particle pairs. A similar application is the calculation of the rate of production of pairs of particles, and the rate of production of massive particles. One example, $K\bar{K}$ production, is shown in Fig. 3.9. For large masses, the weight factor becomes approximately $\exp(-M/T)\approx\exp(-M/T_0)$. Successful predictions range over many orders of magnitude (see Hagedorn, 1970).

Inclusive spectra. As we saw above, the statistical model is very impressive in predicting transverse momentum distributions. When we turn to longitudinal momenta, however, additional assumptions are necessary. Fermi's pure statistical model, which treated transverse and longitudinal momenta on the same footing, could not reproduce the observed forward–backward peaking in the center-of-mass system (Fermi, 1950). Hagedorn and Ranft (1968) overcome this difficulty by assuming that the reaction products emanate not from a single fireball, but from a superposition of fireballs with a continuous distribution of longitudinal velocities. If the superposition were done in terms of the

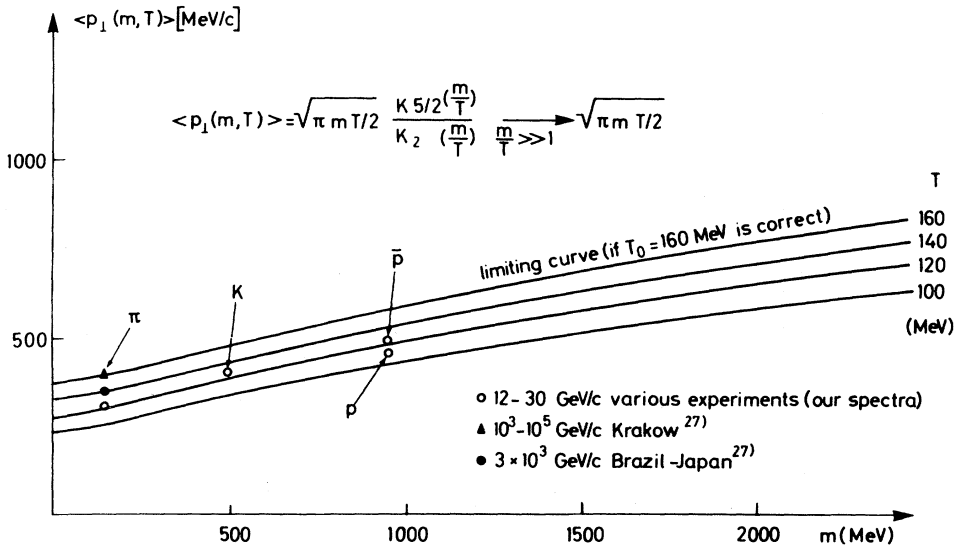

FIG. 3.8. Average transverse momentum predictions of statistical model, compared to cosmic ray data (Hagedorn, 1968a).

rapidity y (actually, Hagedorn and Ranft use a related variable λ), the model for the single-particle inclusive spectrum would be

$$E_q \frac{d^3\sigma}{dq^3} \equiv \rho(q_\perp, q_{||}, s) = \int_0^Y dy\, F(Y, y) L(y) f[E_q', T(y)], \tag{3.40a}$$

where $f(E, T)$ is the Fermi-Dirac or Bose-Einstein distribution,

$$f(E, T) = (e^{E/T} \pm 1)^{-1}, \tag{3.40b}$$

and where $L(y)$ denotes a longitudinal Lorentz transformation on $f(E', T)$. The function $F(Y, y)$ is arbitrary, and is chosen to fit the data.

Since the transverse momentum distribution is unaffected by the superposition, the comments made above about the success of the model are valid. On the

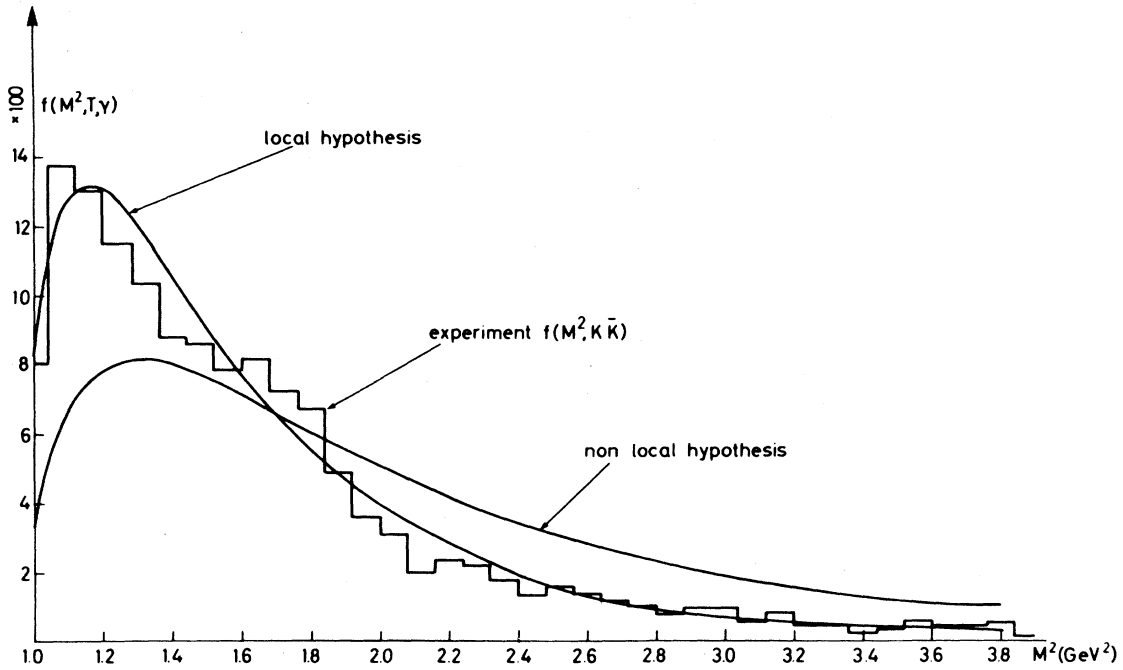

FIG. 3.9. Statistical model predictions for mass spectrum of $K\bar{K}$ pairs Hagedorn, 1968a).

TABLE 4.1 Summary of models, types of experiments, and the predictions made by various models.

Experiment	Model					Beam energy region
	(a) Mueller analysis	(b) Multiperipheral	(c) Diffractive fragmentation	(d) Statistical thermodynamical	(e) Cheng-Wu	
(1) Average multiplicity $\langle n(E)\rangle$	$\langle n(E)\rangle = a \ln E + b$		No prediction; can accommodate any reasonable behavior	$\langle n\rangle$ grows faster than $\ln E$	$\langle n\rangle \propto s^a$, $a>0$	$E>E_p$
(2) Multiplicity distribution $P(n)$	No prediction	Roughly Poisson	$P(n)\propto n^{-2}$ if $\langle n\rangle \propto \ln E$	No prediction	?	$E>E_p$
Partial cross sections $\sigma_n(E)$	No prediction	$(K\ln s)^{n-2}s^{-K}/(n-2)!$, $K=2-2\alpha_M(0)\approx 1$	Constant	No prediction	?	$E>E_p$
(3) One-particle spectra: limiting fragmentation?	Yes	Yes	Yes	Yes	No; $\rho(\mathbf{q})\propto s^a$	$E>E_f$
(4) One-particle spectra: central plateau?	Yes	Yes	No prediction; can be accommodated	Not in present version; can be accommodated	Yes	$E>E_p$
(5) One-particle spectra: factorization in fragmentation regions	Yes	Yes	?	No prediction	?	$E>E_f$
(6) One-particle spectra: factorization in plateau region	Yes	Yes	No	No prediction	?	$E>E_p$
(7) Two-particle spectra: correlations?	Only short-range correlations, if Regge poles≫Regge cuts.		No prediction	No prediction	?	$E>E_f$
(8) Diffraction dissoc. into high missing mass	$\propto g_{PPP}^2$, triple Pomeron coupling	g_{PPP} small or zero	"Favored"	No prediction	?	
(9) $\sigma_{\text{tot}}(E)$	$\sigma\propto$ const. or $s^{-\epsilon}$, $\epsilon\ll 1$.		Constant	No prediction	$\sigma\propto \ln^2 s$	

other hand, the longitudinal momentum distribution is given essentially by $F(Y, y)$, since $f(E, T)$ is peaked at low values of $q_{||}$. Therefore the model is purely phenomenological in this respect. It is consistent with the hypothesis of limiting fragmentation, provided that at high energies $T \to T_0$ and $F(Y, y) \to F(y)$. Successes of the Hagedorn–Ranft model in fitting longitudinal momentum distributions are thus largely tests of ideas which are more general than the specific model; in particular, the fact that limiting fragmentation seems to be fairly well achieved at accelerator energies.

The model as we have formulated it can also satisfy scaling, even at $x=0$. In other language, one can choose $F(y)$ to be flat in the central region. The variable λ actually used by Hagedorn and Ranft is less convenient for this purpose, as DeTar has discussed (DeTar, 1971).

The literature on the statistical thermodynamical model is lengthy. Although we have tried to identify the most impressive successes of the model, we cannot discuss all the intricacies involved in the fine tuning of the model to fit the data. As an introduction to further study, we suggest Frautschi (1971), followed by the review of Ranft and Ranft (1970) and Hagedorn (1970b), at which point the student should be ready for the original literature (Hagedorn and Ranft, 1968; Hagedorn, 1968).

IV. SUMMARY OF MODELS AND TYPES OF EXPERIMENTS

As a guide to help the reader find his way through this review, we shall list the types of experiments which have been discussed most thoroughly, along with the predictions made by the various models. These are given in concise form as a large matrix, Table 4.1. It is necessarily incomplete and oversimplified. An explanation of the terms used in the table follows:

Types of experiments

(1) Average multiplicity: The average number of particles produced, as a function of beam energy. In practice, only charged particles are detected. (Sec. III.A and II.F.)

(2) Partial cross sections and multiplicity distributions: The two-dimensional distribution $\sigma(n, E)$ representing the energy dependence of the cross section to produce n particles ($n>2$). In practice, only $\sigma(n_c, E)$ is measured—the cross section for the production of n_c charged particles plus an unknown number of neutrals. (Section II.F)

(3) Single-particle spectra; limiting fragmentations: Investigation of whether the single-particle spectra approaches constant limits at high beam energy E. (Section II.C)

(4) Single-particle spectra; central plateau: Investigation of whether a central plateau develops in the spectrum as a function of the rapidity y. (Sections II.D.3 and II.E.2)

(5) Single-particle spectra, factorization in fragmentation regions: Investigation of the factorization prediction that the density $\rho_{ab}{}^c(q_\perp, y, y-Y)$ is independent of the projectile in the target fragmentation region, and independent of the target in the projectile fragmentation region. (Sections II.D and II.E.5)

(6) Single-particle spectra, factorization in plateau region: Investigation of the prediction that the normalized spectrum is independent of both the beam and the target in the central region, $\rho_{ab}(q_{||}, q_\perp, y) = \gamma(q_\perp)$. (Sections II.D and II.E.2)

(7) Two-particle spectra, correlations: Exploration of the correlation function in two-particle inclusive reactions. The correlation function is defined as $C^{(2)}(y_1, \mathbf{q}_{1\perp}; y_2, \mathbf{q}_{2\perp}; s) \equiv \rho^{(2)}(y_1, \mathbf{q}_{1\perp}, y_2, \mathbf{q}_{2\perp}; s) - \rho^{(1)}(y_1, q_{1\perp}, s) \times \rho^{(1)}(y_2, q_{2\perp}, s)$. In particular, does there exist a correlation length L, such that for $|y_1 - y_2| \gg L$, $C^{(2)} \approx 0$? (Sections II.D.4 and II.E.7)

(8) Diffraction dissociation into high missing mass: Measurement of diffractive dissociation into high-mass states; which can be interpreted in terms of the "triple-Pomeron" coupling, an important parameter in multiperipheral models. (Sections III.A and II.E.6)

(9) Total cross sections: The simplest multiparticle production experiment, which nevertheless helps discriminate among the models presented.

Models

(a) Mueller analysis: Analysis of multiparticle inclusive reactions via generalized unitarity relations plus assumption of Regge pole dominance of absorptive parts of amplitudes. (Section II.E)

(b) Multiperipheral model: Specifically, multiperipheral models in which exchange of lower-lying trajectories dominates. Internal Pomeron couplings are weak. (Section III.A)

(c) Diffractive fragmentation models: Models in which particle production occurs via separate fragmentation of target and projectile. (Sections III.B)

(d) Statistical-thermodynamic model: The Hagedorn–Ranft model, employing statistical distributions of produced particles. (Section III.D)

(e) Cheng-Wu model: Sum of certain set of Feynman diagrams in high-energy limit. (Section III.C)

Beam energy region

The fragmentation threshold E_f is the beam lab energy above which the ends of the single-particle spectra approach their fragmentation limits. The plateau threshold E_p is the energy above which the central plateau begins to develop.

The speculations in Sec. II.D.2 say that $E_p \propto E_f{}^2$. There is evidence that $E_f \lesssim 10$ GeV (lab energy, nucleon target), and some indication (see Sec. II.D.2) that $30 < E_p \lesssim 200$ GeV.

REFERENCES

Abarhanel, H. D. I. and C. Itzykson, 1969, Phys. Rev. Letters **23,** 53.
——, and L. M. Saunders, 1970, Phys. Rev. **D2,** 711.
——, 1971a, Phys. Rev. **D3,** 2227.
——, 1971b, Phys. Letters **34B,** 69.
——, G. F. Chew, M. L. Goldberger, L. M. Saunders, 1971c, Phys. Rev. Letters **26,** 937.
——, G. F. Chew, M. L. Goldberger, L. M. Saunders, 1971d, Phys. Rev. **D4,** 2988.
——, D. J. Gross, 1971e, Phys. Rev. Letters **26,** 732.
Abolins, M. A., G. A. Smith, Z. M. Ma, E. Gellert, and A. B. Wicklund, 1970, Phys. Rev. Letters **25,** 126.
Akerlof, C. W., D. G. Crabb, J. L. Day, A. D. Krisch, M. T. Lin, L. G. Ratner, and K. W. Edwards, 1967, Phys. Rev. Letters **18,** 1218.
——, D. G. Crabb, J. L. Day, A. D. Krisch, M. T. Lin, L. G. Ratner, and K. W. Edwards, 1968, Phys. Rev. **166,** 1353.
——, D. G. Crabb, J. L. Day, N. P. Johnson, P. Kalbaci, A. D Krisch, M. T. Lin, M. L. Marshak, J. K. Randloph, P. Schmueser, A. L. Read, K. W. Edwards, J. G. Asbury, G. J. Marmer, L. G. Ratner, 1971, Phys. Rev. **D3,** 645.
Akimov, V. N., D. S. Chernavskii, I. M. Dremin, I. I. Royzen, 1969, Nucl. Phys. **B14,** 285.
Allaby, J. V., F. Binon, A. N. Diddens, P. Duteil, A. Klovning, R. Meunier, J. P. Pergneux, E. J. Sacharidis, K. Schlupmann, M. Spighell, J. P. Stroot, A. M. Thorndike, A. M. Wetherell, 1968, Phys. Letters **28B,** 229.
——, F. Binon, A. N. Diddens, P. Duteil, G. Giacomelli, R. Meunier, J. P. Peigneux, K. Schlupmann, M. Spighel, C. A. Stahlbrandt, J. P. Stroot, A. M. Wetherell, Yu. B. Bushnin, S. P. Denisov, S. V. Donskov, A. F. Dunaitsen, Yu. P. Gorin, V. A. Kachanov, Yu. S. Khodirev, V. I. Kotov, V. M. Kutyin, A. I. Petrukhin, Yu. D. Prokoshkin, E. A. Razuvaev, R. S. Shuvalov, and D. A. Stoyanova, 1969, Phys. Letters **29B,** 48.
——, F. Binon, A. N. Diddens, P. Duteil, A. Klovning, R. Meunier, J. P. Peigneux, E. J. Sacharidis, K. Schlupmann, M. Spighel, J. P. Stroot, A. M. Thorndike, A. M. Wetherell, 1970a, CERN preprint #70-12.
——, A. N. Diddens, A. Klovning, K. Schlupmann and A. M. Wetherell, 1970b, Phys. Letters **33B,** 429.
Alturelli, G. R. Brandt, and G. Preparata, 1971, Phys. Rev. Letters **26,** 42.
Amaldi, U., R. Biancastelli, C. Bosio, G. Matthie, J. V. Allaby, A. N. Diddens, R. W. Robinson, A. Klovning, J. Litt, L. S. Rochester, K. Schlupmann, and A. M. Wetherell, 1971, Phys. Letters **34B,** 435.
Amann, R. F., 1971, Phys. Rev. Letters **26,** 1349.
Amati, D., S. Fubini, and A. Stanghellini, 1962, Nuovo Cimento **26,** 896.
Anderson, E. W., E. J. Bleser, G. B. Collins, T. Fujii, J. Menes, F. Turkot, R. A. Carrigan, Jr., R. M. Edelstein, N. C. Hien, T. J. McMahon, and I. Nadelhaft, 1966, Phys. Rev. Letters **16,** 855.
——, E. J. Bleser, G. B. Collins, T. Fujii, J. Menes, F. Turkot, R. A. Carrigan, R. M. Edelstein, N. C. Hien, T. J. McMahon, and I. Nadelhaft, 1967, Phys. Rev. Letters **19,** 198.
——, E. J. Bleser, H. R. Blieden, G. B. Collins, D. Garelick, J. Menes, F. Turkot, D. Birnbaum, R. M. Edelstein, N. C. Hien, T. J. McMahon, J. F. Mucci, and J. S. Russ, 1970, Phys. Rev. Letters **25,** 699.
Anderson, J. A., D. B. Smith, and R. J. Sprafka, 1969, Phys. Rev. Letters **23,** 1064.
Anthony, R. W., C. T. Coffin, E. S. Meanly, J. E. Rice, K. M. Terwilliger, and N. R. Stanton, 1971, Phys. Rev. Letters **26,** 38.
Antipov, Yu. M., S. P. Denisov, S. V. Donskov, Yu. P. Gorin, V. A. Kachanov, V. P. Khromov, V. M. Kutjin, L. G. Landsberg, V. G. Lapshin, A. A. Lebedev, A. G. Morozov, A. I. Petrukhin, Yu. D. Prokoshkin, E. A. Razuvaev, V. I. Rykalin, V. I. Solyanik, D. A. Stoyanova, R. S. Shuvalov, N. K. Vishnevsky, F. A. Yetch, and A. M. Zaytzev, 1971, Phys. Letters **34B,** 164.
Appleton, I. C., M. T. Hogue, and B. C. Rastin, 1971, Nucl. Phys. **B26,** 365.
Arnold, R., 1967, Phys. Rev. **153,** 1523.
——, 1971, Argonne National Laboratory Report ANL/HEP 7139.
Asbury, J. G., Y. Cho, M. Derrick, L. G. Ratner, T. P. Wangler, A. D. Krisch, and M. T. Lin, 1969 Phys. Rev. **178,** 2086.
Bali, N. F., G. F. Chew, and A. Pignotti, 1967, Phys. Rev. Letters **19,** 614.
——, L. S. Brown, R. D. Peccei, and A. Pignotti, 1970a, Phys. Rev. Letters **25,** 557.
——, L. S. Brown, R. D. Peccei, and A. Pignotti, 1970b, Phys. Letters **33B,** 175.
——, A. Pignotti, and D. Steele, 1971, Phys. Rev. **D3,** 1167.
Ball, J. S. and G. Marchesini, 1969a, Phys. Rev. **188,** 2209.
——, and G. Marchesini, 1969b, Phys. Rev. **188,** 2508.
——, and G. Marchesini, 1970, Phys. Rev. **D2,** 2665.
——, and S. Pinsky, 1971, Phys. Rev. Letters **26,** 669.
——, and F. Zachariasen, 1969, Phys. Letters **30B,** 558.
——, and F. Zachariasen, 1971, Phys. Rev. **D3,** 1596.
Bardakci, K. and S. Mandelstam, 1969, Phys. Rev. **184,** 1640.
Benecke, J., T. T. Chou, C. N. Yang and E. Yen, 1969, Phys. Rev. **188,** 2159.
Berestetsky, V. B. and I. Ya. Pomeranchuk, 1961, Nucl. Phys. **22,** 629.
——, and I. Ya. Pomeranchuk, 1961, Sov. Phys. JETP **12,** 752.
Berger, E. L., 1971, Colloquium on Multiparticle Dynamics, Helsinki.
Berman, S. M. and M. Jacob, 1970, Phys. Rev. Letters **25,** 1683.
Bertocchi, L., S. Fubini, and M. Tonin, 1962, Nuovo Cimento **25,** 626.
Białas, A., L. Michejda, and J. Turnau, 1968, Nuovo Cimento **56A,** 241.
——, and L. Van Hove, 1969, Nuclear Physics **B11,** A79.
Bialkowski, G., and R. Sosnowski, 1967, Phys. Letters **25B,** 519.
Binon, F., S. P. Denisov, P. Duteil, V. A. Kachanov, V. M. Kutyin, J. P. Peigneux, Yu. D. Prokoshkin, E. A. Razuvaev, R. S. Shuvalov, M. Spighel, and J. P. Stroot, 1969, Phys. Letters **30B,** 506.
Biswas, N. N., N. M. Cason, V. P. Kennex, J. T. Powers, W. D. Shephard, and D. W. Thomas, 1971, Phys. Rev. Letters **26,** 1589.
Bjorken, J., 1971, Proceedings of the APS Division of Particles and Fields Meeting, Rochester.
Blanckenbecler, R., and R. L. Sugar, 1970, Phys. Rev. **D2,** 3024.
Bloom, E. D., and F. J. Gilman, 1970, Phys. Rev. Letters **25,** 1140.
Boggild, H., E. Dahl-Jensen, K. H. Hansen, J. Johnstad, E. Lohse, M. Suk, L. Veje, V. J. Karimaki, K. V. Laurikainen, E. Riipinen, T. Jacobsen, S. O. Sorensen, J. Allen, G. Blomquist, O. Danielsen, G. Ekspong, L. Granstrom, S. O. Holmgren, S. Nilsson, B. E. Ronove, U. Sredin, and N. K. Yamdagni, 1971a, Nucl. Phys. **B27,** 285.
——, K. H. Hansen, and M. Suk, 1971b, Nucl. Phys. **B27,** 1.
Byckling, E., and K. Kajantie, 1969, Phys. Rev. **187,** 2008.
Byers, N., and C. N. Yang, 1966, Phys. Rev. **142,** 976.
Campbell, J. E., Nuovo Cimento, 1969, **61A,** 307.
Caneschi, L., and A. Schwimmer, 1970, Phys. Letters **33B,** 577.
——, and A. Schwimmer, 1971, Phys. Rev. **D3,** 1588.
——, D. E. Lyon, Jr., and Clifford Risk, 1970, Phys. Rev. Letters **25,** 774.
——, and A. Pignotti, 1969a, Phys. Rev. **184,** 1915.
——, and A. Pignotti, 1969b, Phys. Rev. Letters **22,** 1219.
——, 1969, Lettere al Nuovo Cimento II, 122.
Carlitz, R., M. B. Green, and A. Zee, 1971, Phys. Rev. Letters **26,** 1515.
Chan, H. M., C. S. Hsue, C. Quigg, and J-M. Wang, 1971a, Phys. Rev. Letters **26,** 672.
——, 1968, Proc. Intern. Conf. on High Energy Physics, Vienna, **14,** 391.
——, K. Kajantie, and G. Ranft, 1967, Nuovo Cimento **49,** 157.
——, and P. Hoyer, 1971b, Phys. Letters **36B,** 79.
——, J. Koskiewicz, and W. W. M. Allison, 1968, Nuovo Cimento **57,** 93.
Chang, S. J., and S. K. Ma, 1969, Phys. Rev. Letters **22,** 1334.
——, and S. K. Ma, 1968, Phys. Rev. **180,** 1506.
——, and P. M. Fishbane, 1971, Phys. Rev. **D3,** 1047.
——, and T. M. Yan, 1970, Phys. Rev. Letters **25,** 1586.
——, and T. M. Yan, Univ. of Illinois preprint #71-4.
Chen, M. S., R. R. Kinsey, T. W. Morris, R. S. Panvini, L. L. Wang, T. F. Wong, S. L. Stone, T. Ferbel, P. Slattery, B. Werner, J. W. Elbert and A. R. Erwin, 1971a, Phys. Rev. Letters **26,** 1585.

——, and F. E. Paige, 1971b, Phys. Rev. **D4,** 2163.
Cheng, H., and T. T. Wu, 1970, Phys. Rev. Letters **24,** 1456 (1970).
——, and T. T. Wu, 1971, Phys. Letters **34B,** 647.
——, and T. T. Wu, 1971, Phys. Rev. **D3,** 2195.
Chew, G. F., and A. Pignotti, 1968a, Phys. Rev. Letters **20,** 1078.
——, and A. Pignotti, 1968b, Phys. Rev. **176,** 2112.
——, and W. R. Frazer, 1968, Phys. Rev. **181,** 1914.
——, M. L. Goldberger, and F. E. Low, 1969a, Phys. Rev. Letters **22,** 208.
——, and C. DeTar, 1969b, Phys. Rev. **180,** 1577.
——, and D. Snider, 1971, Phys. Rev. **D3,** 420.
——, and D. R. Snider, 1970a, Phys. Rev. **D1,** 3453.
——, and D. R. Snider, 1970b, Phys. Letters **31B,** 75.
——, T. W. Rogers, and D. R. Snider, 1970, Phys. Rev. **D2,** 765.
Chliapnikov, P., O. Czyzewski, J. Finkelstein, and M. Jacob, 1971, Phys. Letters **35B,** 581.
Chou, T. T., and C. N. Yang, 1968, Phys. Rev. **170,** 1591.
——, and C. N. Yang, 1970, Phys. Rev. Letters **25,** 1072.
——, 1971, Phys. Rev. Letters **27,** 1247.
Ciafaloni, M., and H. Yesian, 1970, Phys. Rev. **D2,** 2500.
——, C. DeTar, and M. N. Misheloff, 1969, Phys. Rev. **188,** 2522.
——, and C. DeTar, 1970, Phys. Rev. **D1,** 2917.
Cicuta, G. M., and R. L. Sugar, 1971, Phys. Rev. **D3,** 970.
Cocconi, G., 1968, Nuovo Cimento **57A,** 837.
——, A. N. Diddens, E. Lillethum, G. Manning, A. E. Taylor, T. G. Walker, and A. M. Wetherell, 1961, Phys. Rev. Letters **7,** 450.
Cohen, D., M. Farber, T. Ferbel, R. Holmes, P. Slattery, S. L. Stone, and B. Werner, Univ. of Rochester Preprint #875–335.
Colleraine, A. P. and U. Nauenberg, 1967, Phys. Rev. **161,** 1387.
Crabb, D. G., J. L. Day, A. D. Krisch, M. T. Lin, M. L. Marshak, J. G. Asbury, L. G. Ratner, and A. L. Read, 1968, Phys. Rev. Letters **21,** 830.
——, J. L. Day, A. D. Krisch, M. T. Lin, M. L. Marshak, J. G. Asbury, L. G. Ratner, and A. L. Read, 1968, Phys. Rev. Letters **21,** 1097.
Czyzewski, O., and K. Rybicki, 1970, Cracow INP Preprint No. 703/ph.
——, 1968, Proc. Intern. Conf. on High-Energy Phys. (Vienna). **14,** 367.
Day, J. L., N. P. Johnson, P. Kalbaci, A. D. Krisch, M. L. Marshak, J. K. Randolph, G. J. Marner, and L. G. Ratner, 1969, Phys. Rev. Letters **23,** 1469.
——, N. P. Johnson, A. D. Krisch, M. L. Marshak, J. K. Randolph, P. Schmueser, G. J. Marmer, and L. G. Ratner, 1969, Phys. Rev. Letters **23,** 1055, 1064.
DeTar, C. E., 1971, Phys. Rev. **D3,** 128.
——, C. E. Jones, F. E. Low, J. Weis, J. E. Young, and C-I. Tan, 1971a, Phys. Rev. Letters **26,** 675.
——, K. Kang, C-I. Tan, and J. H. Weis, 1971b, Phys. Rev. **D4,** 425.
——, D. Z. Freedman, and G. Veneziano, 1971c, Phys. Rev. **D4,** 906.
——, and D. Snider, 1970, Phys. Rev. Letters **25,** 410.
Einhorn, M. B., M. B. Green, and M. A. Virasoro, 1971, Phys. Letters **37B,** 292.
Elbert, J. W., A. R. Erwin, S. Mikamo, D. Reeder, Y. Y.Chen, and W. D. Walker, 1968, Phys. Rev. Letters **20,** 124.
——, A. R. Erwin, W. D. Walker, and J. W. Waters, 1970, Nuclear Phys. **B19,** 85.
——, A. R. Erwin, and W. D. Walker, 1971, Phys. Rev. **D3,** 2042.
Elitzur, M., 1971, Phys. Rev. **D4,** 910.
Ellis, J., J. Finkelstein, P. H. Frampton, and M. Jacob, 1971, Phys. Letters **35B,** 227.
Ellis, W. E., R. R. Kinsey, T. W. Morris, R. S. Panvini, and F. Turkot, 1970, Phys. Letters **32B,** 641.
Fermi, E., 1950, Progr. Theor. Phys. (Kyoto) **5,** 570.
Ferrara, S., and G. Mattioli, 1970, Nuovo Cimento **65A,** 25.
Feynman, R. P., 1969, Phys. Rev. Letters **23,** 1415.
——, *High Energy Collisions* (Gordon and Breach, New York, 1969) p. 237.
Finkelstein, J., 1970, Phys. Rev. **D2,** 1591.
——, and F. Zachariasen, 1971, CERN #1297.
——, and K. Kajantie, 1968, Phys. Letters **26B,** 305.
Foley, K. J., R. S. Jones, S. J. Lindenbaum, W. A. Love, S. Ozaki, E. D. Platner, C. A. Quarles, and E. H. Willen, 1967, Phys. Rev. Letters **19,** 397.
Frautschi, S., 1963, Nuovo Cimento **28,** 409.
——, 1971, Phys. Rev. **D3,** 2821.
——, and B. Margolis, 1969, Nuovo Cimento **56A,** 1155.
Frazer, W. R., and C. H. Mehta, 1969, Phys. Rev. Letters **23,** 258.
——, and C. H. Mehta, 1970, Phys. Rev. **D1,** 696.
——, 1970, in Proc. International Conference on Expectations for Particle Reactions at the New Accelerator, Madison.
——, 1971a, in *Phenomenology in Particle Physics,* edited by C. B. Chiu et al., (Caltech).
——, 1971b, Proceedings of the Hawaii Topical Conference on Particle Physics.
——, C. H. Poon, D. Silverman, and H. J. Yesian, 1971c, University of Calif., Berkeley, preprint.
Freedman, D. Z., C. E. Jones, F. E. Low, and J. E. Young, 1971, Phys. Rev. Letters **26,** 1197.
Freidlander, E., 1966, Nuovo Cimento **41A,** 417.
Friedman, J. H. and C. Risk, UCRL #20278.
——, and C. Risk, LBL-25.
Frodesen, A. G., O. Skjeggestad, and P. Saetre, 1970, Nucl. Phys. **B18,** 45.
Fuji, Z., S. Tida, Y. Kamiya, S. Kawaguchi, and A. Takenaka, 1969, Lettere al Nuovo Cimento, Vol. I, 845.
Fubini, S., and G. Veneziano, 1969a, Nuovo. Cimento **64A,** 811.
——, D. Gordon, and G. Veneziano, 1969b, Phys. Letters **29B,** 679.
——, 1964, in *Strong Interactions and High Energy Physics,* edited by K. G. Moorhouse (Oliver and Boyd, Edinburgh and London).
Goldberger, M. L., C.-I. Tan, and J. M. Wang, 1969, Phys. Rev. **184,** 1920.
——, D. Silverman, and C-I. Tan, 1971, Phys. Rev. Letters **26,** 100.
Gordon, D., and G. Veneziano, 1971, Phys. Rev. **D3,** 2116.
Gribov, V. N., 1967, Zh. Eksp. Teor. Fiz. **53,** 654. [Sov. Phys. JETP **26,** 414 (1968)].
Hagedorn, R., 1965, Nuovo Cimento Supplemento **3,** 147.
——, 1967, Nuovo Cimento **52A,** 1336.
——, and J. Ranft, 1968a, Nuovo Cimento Supplemento **6,** 169.
——, 1968b, Nuovo Cimento Supplemento **6,** 311.
——, 1968, Nuovo Cimento **56A,** 1027.
——, 1970a, Nucl. Phys. **B24,** 93.
——, 1970b, Invited paper at the Colloquium on "High Multiplicity Hadronic Interactions" held at Ecole Polytechnique, Paris, May 13, 1970. Ref. Th. 1174-CERN.
——, 1970c, Astron. and Astrophys. **5,** 184.
Halliday, I. G., 1970, Nucl. Phys. **B21,** 445.
——, 1969a, Nuovo Cimento **60A,** 177.
——, and L. M. Saunders, 1969b, Nuovo Cimento **60A,** 494.
Hasslacher, B., D. K. Sinclair, G. M. Cicuta, and R. L. Sugar, 1970, Phys. Rev. Letters **25,** 1591.
Honecker, R., B. Junkmann, R. Schulte, R. Steinberg, N. Tsanos, J. Klugow, S. Nowak, E. Ryseck, M. Walter, K. Bockmann, H. Drevermann, W. Johnson, K. Sternberger, B. Nagini, H. Bottcher, V. T. Cocconi, J. D. Hansen, G. Kellner, D. R. O. Morrison, K. Paler, A. Mihul, V. Muskaler, T. Coghen, O. Czyzewski, K. Eskreys, J. Loskiewicz, J. Zaorska, S. Brandt, O. Braun, V. Luth, T. P. Shah, H. Wenninger, M. Bardadin-Otwinonska, T. Hofnoki, L. Michejda, S. Otwinowski, R. Sosnowski, M. Szeptycka, W. Wojcik, and A. Wroblewski, 1969, Nucl. Phys. **B13,** 571.
Huang, K., and S. Weinberg, 1970, Phys. Rev. Letters **25,** 895.
Hwa, R. C., 1971, Phys. Rev. Letters **26,** 1143.
——, 1970, Phys. Rev. **D1,** 1790.
Heisenberg, W., 1953, "Theory of Multiple Meson Production", in *Vorträge über Kosmische Strahlung,* translated by L. V. Lindern and B. Stringfellow (Springer, 1970).
Jain, P. L., and R. K. Shipurvi, 1970, Lettere al Nuovo Cimento **3,** 535.
Jones, L. W., A. E. Bussian, G. D. DeMeester, B. W. Loo, D. E. Lyon, Jr., P. V. Ramana Murthy, R. F. Roth, F. E. Mills, J. G. Learned, D. D. Reeder, K. N. Erickson, and B. Cork, 1970, Phys. Rev. Letters **25,** 1679.

Kaiser, G. D., University of Cambridge Preprint HEP 70–8.
Kibble, T. W., 1963, Phys. Rev. **131,** 2282.
Kinsey, R. R., T. W. Morris, and R. S. Panvini, 1970, Brookhaven Preprint #14934.
Kittel, W., S. Ratti, and L. Van Hove, 1971, Nucl. Phys. **B30,** 333.
Ko, W., and R. L. Lander, 1971a, Phys. Rev. Letters **26,** 1064.
——, and R. L. Lander, 1971b, Phys. Rev. Letters **26,** 1284.
Krisch, A., 1971, Proceedings of the APS Division of Particles and Fields Meeting, Rochester.
Krzywicki, A, and O. Pene, 1969b, Nucl. Phys. **B12,** 415.
——, 1969a, Phys. Rev. **187,** 1964.
Kugler, M., H. Lipkin, and V. Rittenberg, Argonne National Lab preprint.
Lander, Richard L., 1971, Proceedings of the APS Division of Particles and Fields Meeting, Rochester.
Levy, M., and J. Sucher, 1969, Phys. Rev. **186,** 1656.
——, and J. Sucher, 1970, Phys. Rev. **D2,** 1716.
Lilund, A., and H. Pilkuhn, Phys. Letters 1969, **29B,** 663.
Lipes, R., G. Zweig, and W. Robertson, 1969, Phys. Rev. Letters **22,** 433.
Lo, S. Y., 1970, Nuovo Cimento Letters **3,** 555.
Logunov, A., M. A. Mestvirishvili, and Nguyen Van Hieu, 1967, Phys. Letters **25B,** 611.
Low, F. E., 1969, Brookhaven National Laboratory 50162–(T527).
Lyon, D. E., Jr., A. E. Bussian, G. D. DeMeester, L. W. Jones, B. W. Loo, P. V. Ramana Murthy, R. F. Roth, F. E. Mills, J. G. Learned, D. D. Reeder, K. N. Erickson, B. Cork, and C. Risk, 1971a, Phys. Rev. Letters **26,** 728.
——, Clifford Risk, and Don Tow, 1971b, Phys. Rev. **D3,** 104.
——, 1970, in Proc. of Symposium on High Energy Interactions and Multiparticle Production, November 1970, Argonne National Lab. ANL/HEP 7107.
Misheloff, M. N., 1971, Phys. Rev. **D3,** 1486.
Mueller, A. H., 1970, Phys. Rev. **D2,** 2963.
——, 1971, Phys. Rev. **D4,** 150.
——, and I. J. Muzinich, 1970a, Annals Phys. **57,** 20.
——, and I. J. Muzinich, 1970b, Annals Phys. **57,** 500.
Muzinich, I. J., G. Tiktopoulos, and S. B. Treiman, 1971, Phys. Rev. **D3,** 1041.
Narayan, D. S., 1968, Phys. Rev. **176,** 2154.
Niedermayer, F., and A. Patkos, May 1971, Budapest Preprint #ITP–290.
Nyborg, P., 1968, in *Kinematics and Multiparticle Systems* (Gordon and Breach, New York), p. 82.
——, 1970, Nuovo Cimento **65A,** 544.
Olesen, P., 1970a, Nucl Phys. **B18,** 459.
——, 1970b, Nucl. Phys. **B19,** 589.
Panofsky, W. K. H., 1968, *Proceedings of 14th International Conf. on High Energy Physics, Vienna,* edited by J. Prentki and J. Steinberger (CERN, Geneva, 1968) p. 23.
Peccei, R. D., and A. Pignotti, 1971, Phys. Rev. Letters **26,** 1076.
Pickup, E., D. K. Robinson, and E. O. Salant, 1962, Phys. Rev. **125,** 2091.
Pignotti, A. and P. Ripa, 1971, Phys. Rev. Letters **27,** 1538.
Pinsky, S., and W. Weisberger, 1970, Phys. Rev. **D2,** 1640.
——, and W. Weisberger, Weizman Institute Preprint 70–91.
——, and W. Weisberger, 1970, Phys. Rev. **D2,** 2365.
Piotrowska, H., 1970, Phys. Letters **32B,** 71.
Poon, C. H., 1970, Nucl. Phys. **B20,** 509.
Popova, A. M. and K. A. Ter-Martirosyan, 1964, Nucl. Phys. **60,** 107.
Quigg, C., 1971, Proceedings of the APS Division of Particles and Fields Meeting, Rochester.
Rajaraman, R., 1970, Phys. Rev. **D1,** 118.
Ranft, J., 1970, Phys. Letters **31B,** 529.
Ranft, G., and J. Ranft, 1970, Lectures delivered to the Symposium on High-Energy Physics, Kühlungsborn, DDR. (Preprint TUL 41, Karl–Marx-Universität, Leipzig, DDR).
Ratner, L., R. Ellis, G. Vannini B. Babcock, A. Krisch, J. Roberts, 1971, Phys. Rev. Letters **27,** 68.
Risk, C., and J. H. Friedman, 1971, Phys. Rev. Letters **27,** 353.
Royzen, I. I. 1969, Phys. Letters **29B,** 428.
Saunders, L. M., O. H. N. Saxton, and C-I. Tan, 1971, Phys. Rev. **D3,** 1005.
Silverman, D., P. D. Ting, and H. J. Yesian, UCSD Report #10P10–81.
——, P. D. Ting, and H. J. Yesian, 1971a, Phys. Letters **35B,** 427.
——, and C-I. Tan, 1971a, Phys. Rev. **D1,** 3479.
——, and Chung-I Tan, 1971b, Phys. Rev. **D2,** 233.
——, and C-I. Tan, 1971b, Phys. Rev. **D3,** 991.
——, and Chung-I. Tan, 1971c, Nuovo Cimento **2A,** 489.
Smith, D. B., R. J. Sprafka, and J. A. Anderson, 1969, Phys. Rev. Letters **23,** 1064.
Smith, Dennis B., 1971, Ph.D. thesis, University of California, (UCRL–20632), Berkeley.
Snider, D. R. and D. M. Tow, 1971, Phys. Rev. **D3,** 996.
Stapp, H. P., 1971, Phys. Rev. **D3,** 3177.
Stone, S., T. Ferbel, P. Slattery, and B. Werner, 1971, Univ. of Rochester preprint #UR-875-349.
Suranyi, P., 1971, Phys. Letters **35B,** 169.
Tan, Chung-I., 1971a, Brown University Preprint.
——, 1971b Phys. Rev. **D3,** 790.
Ter-Martirosyan, K. A., 1963, Sov. Phys. JETP **17,** 233.
——, 1964, Nucl. Phys. **68,** 591.
Tiktopoulos, G., and S. B. Treiman, 1971, Phys. Rev. **D3,** 1037.
Ting, P. D., 1970, Phys. Rev. **D2,** 2982.
——, and H. J. Yesian, 1971, Phys. Letters **35B,** 321.
——, 1969, Phys. Rev. **181,** 1942.
Toller, M., 1965, Nuovo Cimento **37,** 631.
Tow, Don M., 1970, Phys. Rev. **D2,** 154.
Van Der Velde, J. C., 1970, Phys. Letters **32B,** 501.
Van Hove, L., 1969, Nuclear Physics **B9,** 331.
——, 1971, Physics Reports **1C,** 347.
Veneziano, G., 1971, MIT Preprint #188.
——, 1971, Phys. Letters **34B,** 59.
Walker, W. D., *et al.*, 1970, Nucl. Phys. **B19,** 85.
——, 1969, in *High Energy Collisions* (Gordon and Breach, New York).
Wang, C. L., 1970, Phys. Rev. Letters **25,** 1068.
Wang, C. P., 1969a, Phys. Rev. **180,** 1463.
——, 1969b, Nuovo Cimento **64A,** 546.
——, 1969c, Phys. Letters **30B,** 115.
——, 1970, Phys. Letters **32B,** 125.
Wang, J. M., and L. L. Wang, 1971, Phys. Rev. Letters **26,** 1287.
White, A. R. 1971, Phys. Letters **35B,** 175.
Wilson, K. G., 1963, Acta. Phys. Austr. **17,** 37.
——, 1970, Cornell Preprint CLNS–31.
Wroblewski, A., 1970a, Rapporteur's Talk, Proceedings of 15th International Conference on High Energy Phys. Kiev, U.S.S.R.
——, 1970b, Phys. Letters **32B,** 145.
Wu, T. T., and C. N. Yang, 1965, Phys. Rev. **137,** B708.
Yen, E., and E. L. Berger, 1970, Phys. Rev. Letters **24,** 695.
Yesian, H. J., 1969, Phys. Rev. **187,** 2279.
Zachariasen, F., and G. Zweig, 1967a, Phys. Rev. **160,** 1322.
——, and G. Zweig, 1967b Phys. Rev. **160,** 1326.
——, 1971a, Physics Reports **2C,** 1.
——, 1971b, CERN Reprint TH 1290.
Zuminski, A., 1969, Nucl. Phys. **B14,** 75.